Canadian Mineralogist
Vol. 29, pp. 707-739 (1991)

ORGANIC/INORGANIC REACTIONS IN METAMORPHIC PROCESSES

HAROLD C. HELGESON
Department of Geology and Geophysics, University of California, Berkeley, California 94720, U.S.A.

FOREWORD

This paper is dedicated to Hugh Greenwood in appreciation for all he has so elegantly done to enhance our quantitative understanding of metasomatic processes. It was Hugh Greenwood who first explained how $T\text{-}X_{(CO_2)}$ diagrams can be used to advantage in representing and interpreting complex phase relations in metamorphic systems (Greenwood 1962). I hope he will find Figure 15 in the present communication gratifying in this regard, because to my knowledge it is the first $T\text{-}X_{(CO_2)}$ diagram to be published in which one of the curves represents metastable equilibrium among minerals, a CO_2–H_2O fluid, and hydrocarbon species in petroleum at high temperatures and pressures. I would like to take this opportunity to publicly express my appreciation to Hugh for all he has done for me over the years. I particularly appreciate his thoughtful, incisive, and perceptive contributions to all of the many stimulating discussions we have had. Hugh is always up for just about anything, and we've tested together many organic/inorganic fluids over the years in a determined effort to better understand our mutual perceptions of the world of metamorphic petrology. Through it all, Hugh has been a staunch supportive friend whom I shall miss greatly as an academic colleague, but look forward to seeing often on the ski slopes and sailboats of the future. Thank you, Hugh, for sharing with us over the past 30 years or so your unselfish friendship, challenging intellect, superb craftsmanship, and unparalleled scholarship.

ABSTRACT

Although the ultimate fate of carbon derived from buried biomass during prograde metamorphism of crustal rocks is carbon dioxide, methane, or graphite, geological observations and experimental data reported in the literature suggest that organic compounds in intermediate oxidation states may persist at high temperatures and pressures in hydrocarbon liquids and aqueous solutions over substantial periods of geological time. Thermodynamic calculations indicate that under these circumstances, metastable equilibrium may be achieved in metasomatic processes among certain hydrocarbon species in petroleum and oxidized aqueous species such as CH_3COOH and CO_2 in hydrothermal solutions coexisting with minerals in the system $KAlO_2$–SiO_2–CaO–FeO–H_2S–O–CO_2–H_2O. The calculations reveal that progressive burial of sediments containing hydrocarbon reservoirs or source rocks in which hydrocarbon species in petroleum are in metastable equilibrium with minerals and oxidized carbon-bearing aqueous species favors precipitation of K-feldspar, calcite, and pyrrhotite at the expense of the annite component of biotite, pyrite, siderite (or other Fe-carbonates), and hydrocarbon species in crude oil. The process leads to enrichment of the aqueous phase in CO_2, which reaches a maximum mole fraction of ~0.75 at 320°C. Metastable persistence of crude oil at higher temperatures is probably limited to heavy aromatic-rich crude oils and asphaltenes coexisting with CO_2-rich aqueous fluids in rocks that are devoid of phase assemblages that are capable of buffering the fugacity of oxygen. The calculations also indicate that tectonic release of CO_2-rich fluids from depths in excess of ~10 km may result in precipitation of hydrocarbon liquids as the fluid flows upward toward the surface.

Keywords: organic/inorganic reactions, petroleum, metamorphism, phase relations in the system $KAlO_2$–SiO_2–CaO–FeO–H_2S–O–CO_2–H_2O, hydrocarbons, carbon dioxide, oxygen fugacity.

SOMMAIRE

Le carbone dérivé de matériaux biogéniques enfouis, suite au métamorphisme prograde de roches crustales, apparaît éventuellement sous forme de gaz carbonique, méthane ou graphite; cependant, les observations géologiques et les données expérimentales citées dans la littérature font penser que les composés organiques des niveaux d'oxydation intermédiaires pourraient persister jusqu'à une température et une pression élevées dans des hydrocarbures liquides et des solution aqueuses, et ce, sur une très longue échelle de temps. Les calculs thermodynamiques indiquent que dans de telles circonstances, un équilibre métastable pourrait être atteint au cours des processus métasomatiques impliquant les espèces hydrocarburées dans le pétrole et les espèces aqueuses oxydées telles que CH_3COOH et CO_2, dans les solutions hydrothermales qui coexistent avec les minéraux du système $KAlO_2$–SiO_2–CaO–FeO–H_2S–O–CO_2–H_2O. D'après les calculs, l'enfouissement progressif des sédiments contenant des réservoirs d'hydrocarbures ou des roches-mères dans lesquelles des espèces hydrocarburées du pétrole sont en équilibre métastable avec des minéraux et

des espèces contenant carbone oxydé favorise la précipitation de feldspath potassique, calcite et pyrrhotite aux dépens du pôle annite de la biotite, pyrite, sidérite (ou autre carbonate ferrifère), et des espèces hydrocarburées dans le mazout. Ce processus mène à un enrichissement de la phase aqueuse en CO_2, qui atteint une fraction molaire maximum d'environ 0.75 à 320°C. La persistence métastable du mazout à des températures plus élevées est tout probablement limitée aux mazouts riches en composés lourds aromatiques et aux asphaltènes qui coexistent avec un fluide aqueux riche en CO_2 dans des roches sans phases aptes à tamponner la fugacité de l'oxygène. Les calculs indiquent aussi que la libération tectonique des fluides riches en CO_2 à une profondeur dépassant 10 km pourrait causer la précipitation d'hydrocarbures liquides à mesure que la phase fluide migre vers la surface.

(Traduit par la Rédaction)

Mots-clés: réactions organique–inorganique, pétrole, métamorphisme, relations de phase, système $KAlO_2$–SiO_2–CaO–FeO–H_2S–O–CO_2–H_2O, hydrocarbures, gaz carbonique, fugacité de l'oxygène.

INTRODUCTION

Organic molecules in kerogen, petroleum, and aqueous solutions in the Earth's crust are commonly assumed to be unstable at high temperatures. According to the conventional view of catagenesis (Tissot & Welte 1984, Hunt 1979, North 1985), thermal degradation of kerogen with increasing burial leads to the formation of petroleum at temperatures from ~60° to 120° or, in some cases, at temperatures to 150°C. With further burial and increasing temperature to ~200°C, organic metamorphism (metagenesis) is thought to result in conversion of all organic matter that remains in the sediment to graphite and natural gas consisting primarily of methane. Although attractive from many points of view, this overall scenario has come into question in recent years, primarily in response to mounting evidence that kerogen may retain hydrocarbon-generating potential at much higher temperatures and that under certain circumstances, liquid hydrocarbons may persist metastably at temperatures in excess of 400°C (Simoneit *et al.* 1981, Reverdatto *et al.* 1984, Price *et al.* 1986, Price 1991).

Both catagenesis and metagenesis are essentially processes of progressive deoxygenation of organic material. Thermodynamic calculations indicate that both the Gibbs free energies and enthalpies of the deoxygenation reactions are negative (Sato 1990). Hence, the reactions are favored thermodynamically, but to a decreasing extent with increasing temperature! Nevertheless, the dramatic decrease in oxygen fugacity with increasing depth of burial in the upper few kilometers of a sedimentary basin (Helgeson 1992) results in large chemical affinities for the deoxygenation reactions. The chemical affinity (**A**) of a reaction is given by $\mathbf{A} = RT \ln (K/Q)$, where K and Q stand for the equilibrium constant and activity quotient for the reaction, respectively. Because the second law of thermodynamics requires $\mathbf{A}\, d\xi/dt \geq 0$, where $d\xi/dt$ represents the reaction rate (Prigogine & Defay 1954), it follows that the deoxygenation reactions are favored during catagenesis to an increasing degree with increasing depth of burial to ~3 km (see below), despite their exothermic nature. However, if the oxygen fugacity of the system is buffered at depths in excess of ~3 km by mineral assemblages, the oxygen fugacity will increase with further burial and increasing temperature above ~100°C (Helgeson 1992), which thermodynamically favors preservation of oxidized organic species and inhibition of the deoxygenation reactions at greater depths. As emphasized by Sato (1990), the role of increasing temperature with depth of burial is restricted to increasing exponentially the rates of the deoxygenation reactions. Although the extent to which each of the reaction rates is affected by increasing temperature remains to be determined, recent isotopic data (Peter *et al.* 1991), as well as hydrous pyrolysis experiments and organic geochemistry studies of rocks from ultradeep wells (Price 1983, 1991), indicate that the overall process is rapid in the context of geological time. It thus seems highly unlikely from a thermodynamic point of view that all of the myriad of organic compounds in sedimentary basins would fail to survive burial temperatures in excess of ~150°–200°C.

If stable equilibrium is achieved in metamorphic processes at crustal pressures and temperatures, thermodynamic calculations indicate that all of the carbon in the system C–H–O would be distributed among CH_4, CO_2, and graphite (see below). Hydrothermal precipitation of graphite in metamorphic rocks has received considerable attention in recent years (Dobner *et al.* 1978, Weis *et al.* 1981, Rumble *et al.* 1986, 1989, Rumble & Hoering 1986), but so far CH_4 and CO_2 are the only carbon-bearing species considered in geochemical models that have been invoked to account for the precipitation process. Nevertheless, recent kinetic studies of the decarboxylation of aqueous acetic acid to form CH_4 and CO_2 (Drummond & Palmer 1986, Palmer & Drummond 1986) suggest that aqueous species with intermediate oxidation states between CH_4 and CO_2 may persist at high temperatures over long periods of geological time. This observation is consistent with the high concentrations of carboxylic acids in oil-field brines (Willey *et al.* 1975, Kharaka *et al.* 1977, 1986, Carothers & Kharaka 1978, Workman

& Hanor 1985, Hanor & Workman 1986, Crossey *et al.* 1986, Fisher 1987, Means & Hubbard 1987, MacGowan & Surdam 1987, 1988, 1990a, b, Barth 1991). Analytical data and thermodynamic calculations also indicate that oil-field brines may serve as ore-forming solutions (Sverjensky 1984) and that CO_2 and aqueous carboxylic acids are in homogeneous equilibrium in these brines, but that methane is not (Shock & Helgeson 1986, Shock 1987, 1988, Helgeson & Shock 1988, Helgeson 1991, Helgeson *et al.* 1991).

The temperature limits at which various organic aqueous species become labile has yet to be established, but several lines of evidence suggest that in many instances, these limits are much higher than those considered "reasonable" by organic chemists. For example, a recent thermodynamic analysis (Shock 1990a) of high-temperature experimental data reported by Miller & Bada (1988) indicates that metastable equilibrium among oxidized organic aqueous species may occur at high temperatures. In this case, the species considered were amino acids at 250°C and 260 atmospheres. The high-temperature metastability of organic species is consistent with fluid-inclusion data (Levine *et al.* 1991), as well as the presence of such species in submarine hydrothermal vent waters (Simoneit 1990, 1991, Simoneit *et al.* 1990) and high-temperature springs and fumaroles at Yellowstone National Park (Des Marais & Truesdell 1991). Thermodynamic calculations of the relative stabilities of aqueous peptides, amino acids, and other biochemical molecules (Shock 1988, 1990a, b, c, 1991, Amend & Helgeson 1991) indicate that increasing temperature not only favors the metastable persistence of organic species in oil-field brines, but also the presence of bacteria in hydrocarbon reservoirs.

Liquid hydrocarbons have been found as inclusions in metamorphic minerals formed at ~6 kbar and 300°C (Goffé & Villey 1984) and observed in rock samples retrieved from well depths at which the present-day temperatures range from 225° to 300°C (Price *et al.* 1979, 1981, Price 1982). In his review of evidence for the thermal stability of organic compounds, Shock (1990c) concluded that various organic compounds are preserved in the Earth at temperatures and pressures extending to *at least* 500°C and 10 kbar, depending on the compound.

The role of petroleum, oil-field brines, and organic/inorganic reactions among minerals and fluids in metamorphic processes has yet to be investigated from a thermodynamic point of view. A preliminary step in this direction is represented by the present communication, the purpose of which is to explore with the aid of thermodynamic calculations to what extent organic species in petroleum may be in metastable equilibrium with minerals and oxidized aqueous species during prograde metamorphism of hydrocarbon reservoirs and source rocks in sedimentary basins.

Calculation of Equilibrium Constants at High Temperatures and Pressures for Reactions Involving Minerals, CO_2 Gas, Organic and Inorganic Aqueous Species, and Organic Molecules in Petroleum and Natural Gas

The apparent standard partial molal Gibbs free energy of formation ($\Delta\overline{G}^\circ$) of a given species at a specified pressure (P) and temperature (T) is defined by

$$\Delta\overline{G}^\circ \equiv \Delta\overline{G}^\circ_f + \left(\overline{G}^\circ_{P,T} - \overline{G}^\circ_{P_r,T_r}\right) \tag{1}$$

where $\Delta\overline{G}^\circ_f$ refers to the standard partial molal Gibbs free energy of formation of the species from the elements in their stable form at a reference pressure (P_r) and temperature (T_r) of 1 bar and 298.15 K, and $\overline{G}^\circ_{P,T} - \overline{G}^\circ_{P_r,T_r}$ stands for the difference in the standard partial molal Gibbs free energy of the species at the pressure and temperature of interest, and that at P_r and T_r. The standard state adopted in the present study for minerals, liquid H_2O, and organic species in petroleum is one of unit activity of the thermodynamic components of stoichiometric minerals and pure liquids at any pressure and temperature. The standard state for aqueous species other than H_2O calls for unit activity of the species in a hypothetical one molal solution referenced to infinite dilution at any pressure and temperature. For the thermodynamic components of gases, the standard state is specified as unit fugacity of the pure hypothetical ideal gas at 1 bar and any temperature.

The last term on the right side of Eqn. (1) can be expressed as a function of temperature and pressure by writing

$$\overline{G}^\circ_{P,T} - \overline{G}^\circ_{P_r,T_r} = -\overline{S}^\circ_{P_r,T_r}(T-T_r) + \int_{T_r}^{T} \overline{C}^\circ_{P_r} dT - T\int_{T_r}^{T} \overline{C}^\circ_{P_r} d\ln T + \int_{P_r}^{P} \overline{V}^\circ_T dP \tag{2}$$

where $\overline{S}^\circ_{P_r,T_r}$, $\overline{C}^\circ_{P_r}$, and $\overline{V}^\circ_T$, denote the standard partial modal entropy, heat capacity, and volume of the species at the subscripted pressure and temperature. Equations representing $\overline{C}^\circ_{P_r}$ and $\overline{V}^\circ_T$ in Eqn. (2) are summarized below for minerals, CO_2 gas, aqueous species, and hydrocarbon liquids and gases.

Minerals and CO_2 gas

The standard partial molal heat capacities of minerals and CO_2 gas can be calculated as a function of temperature at 1 bar from power functions used to regress experimental calorimetric data such as those adopted by Maier & Kelley (1932) and Kelley (1960), Haas & Fisher (1976), Berman & Brown (1985), Fei & Saxena (1987), Holland & Powell (1990), and others. The Maier–Kelley power function is sufficiently accurate for use in the present study. It can be expressed as

$$\overline{C}^{\circ}_{P_r} = a + bT + \frac{c}{T^2} \tag{3}$$

where a, b, and c stand for temperature–pressure-independent coefficients characteristic of the mineral. Because the standard partial molal expansibilities $[(\partial\overline{V}^{\circ}/\partial T)_P]$ and compressibilities $[(\partial\overline{V}^{\circ}/\partial P)_T]$ of minerals in the crust of the Earth are small and have an opposing effect on the standard partial molal volumes of minerals with increasing temperature and pressure, $\overline{V}^{\circ}_T$ for most such minerals in Eqn. (2) can be expressed as

$$\overline{V}^{\circ}_T = \overline{V}^{\circ}_{P_r,T_r} \tag{4}$$

without introducing undue uncertainty in calculated values of $\overline{G}^{\circ}_{P,T} - \overline{G}^{\circ}_{P_r,T_r}$ at pressures $\leq$ 10 kbar. Equations (3) and (4) permit Eqn. (2) to be written as

$$\overline{G}^{\circ}_{P,T} - \overline{G}^{\circ}_{P_r,T_r} = -\overline{S}^{\circ}_{P_r,T_r}(T-T_r) + a\left(T - T_r - T\ln\left(\frac{T}{T_r}\right)\right) - \left(\frac{\left(c+bT_r^2T\right)(T-T_r)^2}{2T_r^2T}\right) + \overline{V}^{\circ}_{P_r,T_r}(P-P_r) \tag{5}$$

which can be substituted in Eqn. (1) to generate values of $\Delta\overline{G}^{\circ}$ for minerals. In the case of CO_2 gas, the standard state for gases adopted in the present study (see above) requires $\overline{V}^{\circ}_T$ and $\overline{V}^{\circ}_{P_r,T_r}$ in Eqns. (2) and (5) to be equal to zero.

Aqueous species

The standard partial molal heat capacities and volumes of charged aqueous species as functions of temperature and pressure can be computed from the revised HKF (Helgeson *et al.* 1981) equations of state (Tanger & Helgeson 1988), which can be written as

$$\overline{C}^{\circ}_P = c_1 + \frac{c_2}{(T-\Theta)^2} - \left(\frac{2T}{(T-\Theta)^3}\right)\left(a_3(P-P_r) + a_4\ln\left(\frac{\Psi+P}{\Psi+P_r}\right)\right) + \omega TX + 2TY\left(\frac{\partial\omega}{\partial T}\right)_P - T\left(\frac{1}{\varepsilon}-1\right)\left(\frac{\partial^2\omega}{\partial T^2}\right)_P \tag{6}$$

and

$$\overline{V}^{\circ} = a_1 + \frac{a_2}{\Psi+P} + \frac{a_3}{T-\Theta} + \frac{a_4}{(\Psi+P)(T-\Theta)} - \omega Q + \left(\frac{1}{\varepsilon}-1\right)\left(\frac{\partial\omega}{\partial P}\right)_T \tag{7}$$

where Q, Y, and X denote the partial derivatives of the reciprocal dielectric constant of H_2O (ϵ) given by

$$Q \equiv -\left(\frac{\partial\left(\frac{1}{\varepsilon}\right)}{\partial P}\right)_T = \frac{1}{\varepsilon}\left(\frac{\partial\ln\varepsilon}{\partial P}\right)_T \tag{8}$$

$$Y \equiv -\left(\frac{\partial\left(\frac{1}{\varepsilon}\right)}{\partial T}\right)_P = \frac{1}{\varepsilon}\left(\frac{\partial\ln\varepsilon}{\partial T}\right)_P \tag{9}$$

and

$$X \equiv \left(\frac{\partial Y}{\partial T}\right)_P = \frac{1}{\varepsilon^2}\left[\left(\frac{\partial^2\varepsilon}{\partial T^2}\right)_P - \frac{2}{\varepsilon}\left(\frac{\partial\varepsilon}{\partial T}\right)_P^2\right] \tag{10}$$

$\overline{C}^{\circ}_P$ and $\overline{V}^{\circ}$ refer to the conventional standard partial molal heat capacity and volume of the aqueous species, a_1, a_2, a_3, a_4, c_1, and c_2 represent temperature- and pressure-independent coefficients characteristic of the species, Θ and Ψ stand for solvent parameters equal to 228 K and 2600 bars, respectively, ω designates the conventional Born coefficient of the species, which can be expressed for the jth such species as

$$\omega = \eta\left(Z_j^2\left(r_{e,j,P_r,T_r} + |Z_j|g\right)^{-1} - Z_j(3.082+g)^{-1}\right) \tag{11}$$

where r_{e,j,P_r,T_r} refers to the effective electrostatic radius of the species at the reference pressure and temperature, which for monatomic ions is given by (Helgeson & Kirkham 1976)

$$r_{e,j,P_r,T_r} = r_{x,j} + |Z_j|k_Z \tag{12}$$

and for other charged aqueous species by (Shock *et al.* 1989)

$$r_{e,j,P_r,T_r} = \frac{Z_j^2\left(\eta Y_{P_r,T_r} - 100\right)}{\overline{S}^{\circ}_{j,P_r,T_r} - \alpha_Z} \tag{13}$$

where Z_j stands for the charge on the jth aqueous species, $r_{x,j}$ denotes the crystal radius of the species, η = 1.66027 × 10^5 Å cal mol^{-1}, k_Z designates a constant equal to 0.94 Å for cations and zero Å for anions, g represents a solvent function of temperature and density given by Shock *et al.* (1992), $\overline{S}^{\circ}_{j,P_r,T_r}$ refers to the standard partial molal entropy of the jth aqueous species at the subscripted pressure and temperature, and α_Z is defined by

$$\alpha_Z \equiv 71.5|Z_j| \tag{14}$$

Differentiating Eqn. (11) leads to

$$\left(\frac{\partial \omega}{\partial P}\right)_T = \left(\frac{\partial g}{\partial P}\right)_T X_1 \tag{15}$$

$$\left(\frac{\partial \omega}{\partial T}\right)_P = \left(\frac{\partial g}{\partial T}\right)_P X_1 \tag{16}$$

and

$$\left(\frac{\partial^2 \omega}{\partial T^2}\right)_P = \left(\frac{\partial g}{\partial T}\right)_P^2 X_2 + \left(\frac{\partial^2 g}{\partial T^2}\right)_P X_1 \tag{17}$$

where

$$X_1 \equiv -\eta\left(|Z_j^3|\left(r_{e,j,P_r,T_r} + |Z_j|g\right)^{-2} - Z_j(3.082+g)^{-2}\right) \tag{18}$$

and

$$X_2 \equiv 2\eta\left(Z_j^4\left(r_{e,j,P_r,T_r} + |Z_j|g\right)^{-3} - Z_j(3.082+g)^{-3}\right) \tag{19}$$

Evaluating the integrals in Eqn. (2) with the aid of Eqns. (6)–(19) leads to

$$\begin{aligned}\overline{G}^\circ_{P,T} - \overline{G}^\circ_{P_r,T_r} = &-\overline{S}^\circ_{P_r,T_r}(T-T_r) - c_1\left(T\ln\left(\frac{T}{T_r}\right) - T + T_r\right) \\ &+ a_1(P-P_r) + a_2\ln\left(\frac{\Psi+P}{\Psi+P_r}\right) \\ &- c_2\left(\left(\left(\frac{1}{T-\Theta}\right)-\left(\frac{1}{T_r-\Theta}\right)\right)\left(\frac{\Theta-T}{\Theta}\right) - \frac{T}{\Theta^2}\ln\left(\frac{T_r(T-\Theta)}{T(T_r-\Theta)}\right)\right) \\ &+ \left(\frac{1}{T-\Theta}\right)\left(a_3(P-P_r) + a_4\ln\left(\frac{\Psi+P}{\Psi+P_r}\right)\right) \\ &+ \omega\left(\frac{1}{\varepsilon}-1\right) - \omega_{P_r,T_r}\left(\frac{1}{\varepsilon_{P_r,T_r}}-1\right) + \omega_{P_r,T_r}Y_{P_r,T_r}(T-T_r)\end{aligned} \tag{20}$$

which can be combined with Eqn. (1) to calculate values of ΔG° for ionic aqueous species at high temperatures and pressures.

The analog of Eqn. (20) for neutral aqueous species can be written as (Shock *et al.* 1989, Shock & Helgeson 1990)

$$\begin{aligned}\Delta\overline{G}^\circ = &-\overline{S}^\circ_{P_r,T_r}(T-T_r) - c_1\left(T\ln\left(\frac{T}{T_r}\right) - T + T_r\right) \\ &+ a_1(P-P_r) + a_2\ln\left(\frac{\Psi+P}{\Psi+P_r}\right) \\ &- c_2\left(\left(\left(\frac{1}{T-\Theta}\right)-\left(\frac{1}{T_r-\Theta}\right)\right)\left(\frac{\Theta-T}{\Theta}\right) - \frac{T}{\Theta^2}\ln\left(\frac{T_r(T-\Theta)}{T(T_r-\Theta)}\right)\right) \\ &+ \left(\frac{1}{T-\Theta}\right)\left(a_3(P-P_r) + a_4\ln\left(\frac{\Psi+P}{\Psi+P_r}\right)\right) \\ &+ \omega_e\left(Y_{P_r,T_r}(T-T_r) + \frac{1}{\varepsilon} - \frac{1}{\varepsilon_{P_r,T_r}}\right)\end{aligned} \tag{21}$$

where ω_e denotes the effective Born coefficient of the species, which is independent of pressure and temperature and consistent with

$$\omega_e = \hat{a} + \hat{b}\,\overline{S}^\circ_{P_r,T_r} \tag{22}$$

where $\hat{a}$ and $\hat{b}$ stand for correlation parameters for various groups of neutral aqueous species given by Shock *et al.* (1989), Shock & Helgeson (1990), and D.A. Sverjensky, E.L. Shock, and H.C. Helgeson (in prep.). Equation (21) can be used together with Eqn. (1) to compute apparent standard partial molal Gibbs free energies of formation of both inorganic and organic neutral aqueous species at high temperatures and pressures.

Hydrocarbon liquids

The standard partial molal heat capacities of a large number of organic liquids, gases, and solids can be computed as a function of temperature at one bar from equations given by H.C. Helgeson & A.M. Knox (in prep.), who demonstrated that Eqn. (3) represents closely all of the available heat capacity data for hydrocarbon liquids. However, the c coefficient in Eqn. (3) is positive for hydrocarbon liquids, which is generally not the case for minerals.

The standard partial molal volumes of hydrocarbon liquids at high temperatures and pressures were computed in the present study from the Parameters From Group Contributions (PFGC) equation of state (Cunningham 1974, Majeed & Wagner 1986), which can be written for the standard partial molal compressibility factor ($\overline{z}^\circ$) of a given stoichiometric hydrocarbon as

$$\begin{aligned}\overline{z}^\circ \equiv \frac{P\overline{V}^\circ}{RT} = 1 - \frac{s\overline{V}^\circ}{b}\ln\left(\frac{\overline{V}^\circ - b}{\overline{V}^\circ}\right) - s \\ + 12b^2\sum_i \Psi_i\left(\frac{1-\sum_j \Psi_j\lambda_{ij}}{\overline{V}^\circ - b\left(1-\sum_j \lambda_{ij}\right)}\right)\end{aligned} \tag{23}$$

where R refers to the gas constant, and Ψ_i and Ψ_j stand for the mole fractions of the atoms in the ith and jth polyatomic groups (such as CH_3– and $-CH_2$–) in the hydrocarbon of interest, which are defined for stoichiometric hydrocarbons by

$$\Psi_i = \frac{\nu_i n_i}{\sum_i \nu_i n_i} \tag{24}$$

and

$$\Psi_j = \frac{\nu_j n_j}{\sum_j \nu_j n_j} \tag{25}$$

where ν_i and ν_j denote the stoichiometric number of moles of the ith and jth groups, respectively, in one mole of the hydrocarbon species, and n_i and n_j designate the stoichiometric number of moles of atoms in one mole of the ith and jth groups. The parameters b and s in Eqn. (23) are defined by

$$b \equiv \sum_i \nu_i \overline{V}_i^\circ \tag{26}$$

and

$$s \equiv \sum_i \nu_i n_i s_i \tag{27}$$

where $\overline{V}_i^\circ$ and s_i represent the standard partial molal volume and degree of freedom coefficient of the

ith group, respectively, and λ_{ij} in Eqn. (23) stands for a group-interaction term for the ith and jth groups defined by

$$\lambda_{ij} = \lambda_{ji} \equiv e^{-E_{ij}/kT} \tag{28}$$

where k refers to Boltzmann's constant and

$$E_{ij} \equiv a_{ij}\left(\frac{E_{ii} + E_{jj}}{2}\right) \tag{29}$$

where a_{ij} represents the interaction coefficient for the ith and jth groups and

$$E_{ii} = E_{ii}^{(0)} + E_{ii}^{(1)}\left(\frac{509.7}{RT} - 1\right) \tag{30}$$

where $E_{ii}^{(0)}$ and $E_{ii}^{(1)}$ denote interaction parameters for the subscripted groups. E_{jj} in Eqn. (29) is given by the analog of Eqn. (30) in which the subscript ii is replaced by jj.

Values of b, s, a_{ij}, $E_{ii}^{(0)}$, $E_{ii}^{(1)}$, $E_{jj}^{(0)}$, and $E_{jj}^{(1)}$ in Eqns. (23), (29), and its analog for E_{ij} (30) have been retrieved for a large number of hydrocarbons and other orhanic molecules by regression of pressure-volume-temperature data at pressures and temperatures to ~350 bars and ~240°C (Cunningham 1974, Majeed & Wagner 1986). Average uncertainties in calculated values of $\overline{V}°$ for the n-alkanes in this pressure-temperature range appear to be of the order of a few percent or less.

The PFGC equation of state is based on empirical modification of Eyring's (1936) lattice theory of liquids (Barker 1963, Wilson 1972). Because its theoretical foundations are independent of temperature and pressure, it was used as a first approximation in the present study to predict values of $\overline{V}°$ for n-alkanes at pressures and temperatures beyond those for which experimental data are available. The integrals of $\overline{V}°_T$ in Eqn. (2) for hydrocarbon liquids were evaluated with the aid of a numerical integration computer routine adopted from Arden & Astill (1970). As indicated above, the standard partial molal heat capacity integrals in Eqn. (2) were evaluated for hydrocarbon liquids with the aid of Eqn. (3), but those for hydrocarbons with boiling temperatures at 1 bar that are lower than the temperature of interest were evaluated for the liquid standard state at high temperatures and pressures by taking into account the standard partial molal heat capacities of both the liquid and gas phases along the integration path.

Hydrocarbon gases

The standard partial molal heat capacity of methane gas as a function of temperature at one bar can be computed from Eqn. (3), but those of other hydrocarbon gases at 1 bar are quadratic functions of temperature from 298.15 to 800 K (H.C. Helgeson & A.M. Knox, in prep.), consistent with

$$\overline{C}_{P_r} = \tilde{a} + \tilde{b}T + \tilde{c}T^2, \tag{31}$$

where $\tilde{a}$, $\tilde{b}$, and $\tilde{c}$ stand for constants characteristic of hydrocarbon gases other than methane. As a consequence of the standard state adopted for gases in the present study (see above),

$$\overline{V}° = 0 \tag{32}$$

for gases. Taking account of Eqns. (31) and (32), Eqn. (2) can thus be written for the standard state for gases as

$$\overline{G}°_{P,T} - \overline{G}°_{P_r,T_r} = -\overline{S}°_{P_r,T_r}(T - T_r) + \hat{a}\left(T - T_r - T\ln\left(\frac{T}{T_r}\right)\right) - \frac{\hat{b}}{2}(T - T_r)^2 - \frac{\hat{c}}{6}\left(T^3 - 3T_r^2T + 2T_r^3\right) \tag{33}$$

Equilibrium constants

The equations summarized above permit calculation of equilibrium constants for reactions among minerals and aqueous, liquid, and gas species from

$$\log K = -\frac{\Delta\overline{G}°_r}{2.303RT} \tag{34}$$

where K stands for the equilibrium constant, R again refers to the gas constant, and $\Delta\overline{G}°_r$ denotes the standard partial molal Gibbs free energy of reaction, which is given by

$$\Delta\overline{G}°_r = \sum_i \hat{n}_{i,r}\Delta\overline{G}°_i \tag{35}$$

where $\hat{n}_{i,r}$ designates the stoichiometric reaction-coefficient of the ith solid, aqueous, liquid, or gas species in the rth reaction, which is positive for products and negative for reactants, and $\Delta\overline{G}°_i$ stands for the apparent standard partial molal Gibbs free energy of formation of the ith species, which is given by an appropriate statement of Eqn. (1).

The equations of state parameters and thermodynamic data at 25°C and 1 bar used in the present study to compute values of log K from Eqns. (1)–(35) were taken from Helgeson *et al.* (1978), Majeed & Wagner (1986), Shock & Helgeson (1988, 1990), Shock *et al.* (1989), and H.C. Helgeson & A.M. Knox (in prep.). The calculations were carried out with the aid of program SUPCRT92 (Johnson *et al.* 1992) using equations taken from Johnson & Norton (1991) to compute values of the density and dielectric constant of H_2O and their partial derivatives. The

g function and its partial derivatives were generated from equations given by Shock *et al.* (1992).

Oxidation/Reduction Equilibria among Organic Molecules, Minerals, and Aqueous Species

Although hydrocarbons are covalently bonded, nominal oxidation states can be assigned to the carbon atoms in the molecule so that any change in oxidation state is equivalent to electron transfer in oxidation/reduction reactions. In contrast to reactions among ionic species of different charge, oxidation/reduction reactions involving hydrocarbons or other organic molecules involve incomplete transfer of shared electrons in the covalent carbon bonds. Nevertheless, nominal oxidation states can be assigned to the carbon atoms in organic molecules. As in the case of minerals, it makes no difference if the nominal oxidation states assigned to the carbon atoms in organic species correspond to physical reality because electrons are always conserved in oxidation/reduction reactions. The only requirement for assigning nominal oxidation states to the covalently bonded carbon atoms in organic molecules is that any reaction of the molecule with H_2O does not change the sum of the nominal oxidation states of the carbon atoms (Hendrickson *et al.* 1970). This requirement is met by assigning to a given carbon atom a nominal charge of -1 for each carbon–hydrogen bond, zero for each carbon–carbon bond, and +1 for each carbon–oxygen, carbon–sulfur, or carbon–nitrogen bond. For example, the middle two carbon atoms in *n*-butane, which can be written as

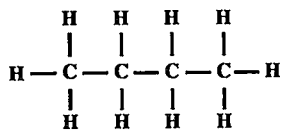

(36)

are assigned nominal oxidation states of -2, but the outer two carbon atoms have a nominal charge of -3. The *average* nominal oxidation state (Z_c) of the carbon atoms in butane is then equal to $[2(-2) + 2(-3)]/4 = -2.5$. Although the law of definite proportions requires the carbon number (n) of organic molecules to be an integer, Z_c and other dependent variables are described below as continuous functions of n, with the implicit understanding that the functions are valid only at integer values of the independent variable. For example, Z_c for *n*-alkanes is plotted in Figure 1 as a function of carbon number for $n = 1,2,\ldots,50$, where the carbon number n represents the stoichiometric number of moles of carbon atoms in one mole of the *n*-alkane chain. It can be deduced from this

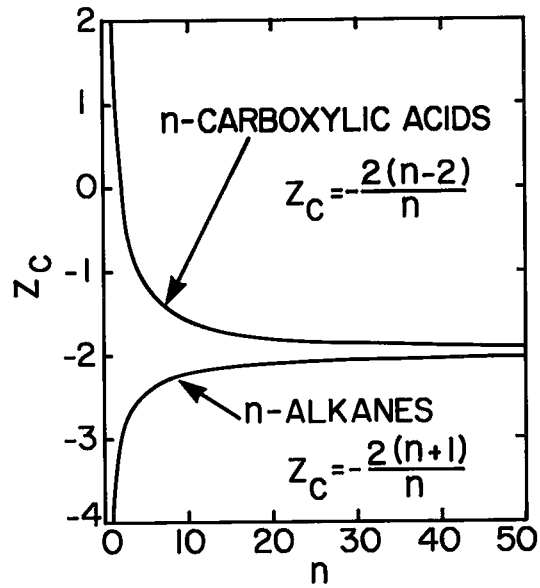

FIG. 1. Average nominal oxidation states of the carbon atoms (Z_c) in *n*-carboxylic acids and *n*-alkanes (see text).

figure that Z_c is an asymptotic function of n for which

$$\lim_{n\to\infty} Z_c = -2 \tag{37}$$

and

$$\lim_{n\to 1} Z_c = -4 \tag{38}$$

Z_c can be regarded as a measure of the relative oxidation states of organic molecules. Although *n*-alkanes become more oxidized with increasing carbon number, alkylbenzenes and oxygen-bearing species such as the carboxylic acids become more reduced. For example, the nominal oxidation state of the carbon atom in formic acid (HCOOH), which corresponds to

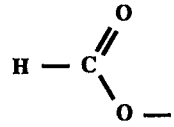

(39)

is 2 because the carbon atom is assigned a charge of 1 for each bond to an oxygen atom. However, the average nominal oxidation state of the carbon atoms in acetic acid (CH_3COOH), which can be idealized as

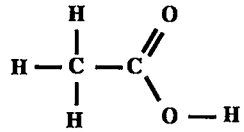

(40)

is zero. Z_c for n-carboxylic acids is plotted in Figure 1 as a function of n for n = 1,2,...,50. It can be seen in this figure that Z_c for the carboxylic acids also is an asymptotic function of carbon number, which approaches the same limit as that of the n-alkanes (-2) as $n \rightarrow \infty$. However, in contrast to the curve for the n-alkanes in Figure 1, Z_c for the n-carboxylic acids approaches 2 as $n \rightarrow 1$. Note that in the case of both curves in Figure 1, 90% of the change in the average nominal oxidation state of the carbon atoms occurs from n = 1 to n = 10. At n greater than or approximately equal to 20, the absolute difference in the average nominal oxidation states of the carbon atoms in n-alkanes and n-carboxylic acids is less than or approximately equal to 0.3.

Acetic acid and its dissociated counterpart (the acetate anion) are apparently the most abundant organic aqueous species in oil-field brines, which are known to contain as much as 10,000 ppm total acetate (MacGowan & Surdam 1988, 1990b). Acetic acid is apparently in metastable equilibrium with aqueous CO_2 and other carboxylic acids in these brines (Shock & Helgeson 1986, Shock 1987, 1988, Helgeson & Shock 1988, Helgeson 1991, Helgeson *et al.* 1991), which is consistent with

$$2CO_{2(aq)} + 2H_2O \rightleftarrows CH_3COOH_{(aq)} + 2O_{2(g)} \qquad (41)$$

where the subscripts (aq) and (g) stand for aqueous and gas states, respectively. The logarithmic analog of the law of mass action for reaction (41) can be written for $a_{H_2O} \approx 1$ as

$$\log a_{CH_3COOH_{(aq)}} = \log K + 2\log a_{CO_{2(aq)}} - 2\log f_{O_{2(g)}} \qquad (42)$$

where K refers to the equilibrium constant for reaction (41), a_{H_2O}, $a_{CH_3COOH(aq)}$, and $a_{CO_2(aq)}$ denote the activities of the subscripted aqueous species, and $\log f_{O_{2(g)}}$ designates the fugacity of oxygen in the system. The assumption of unit activity of H_2O

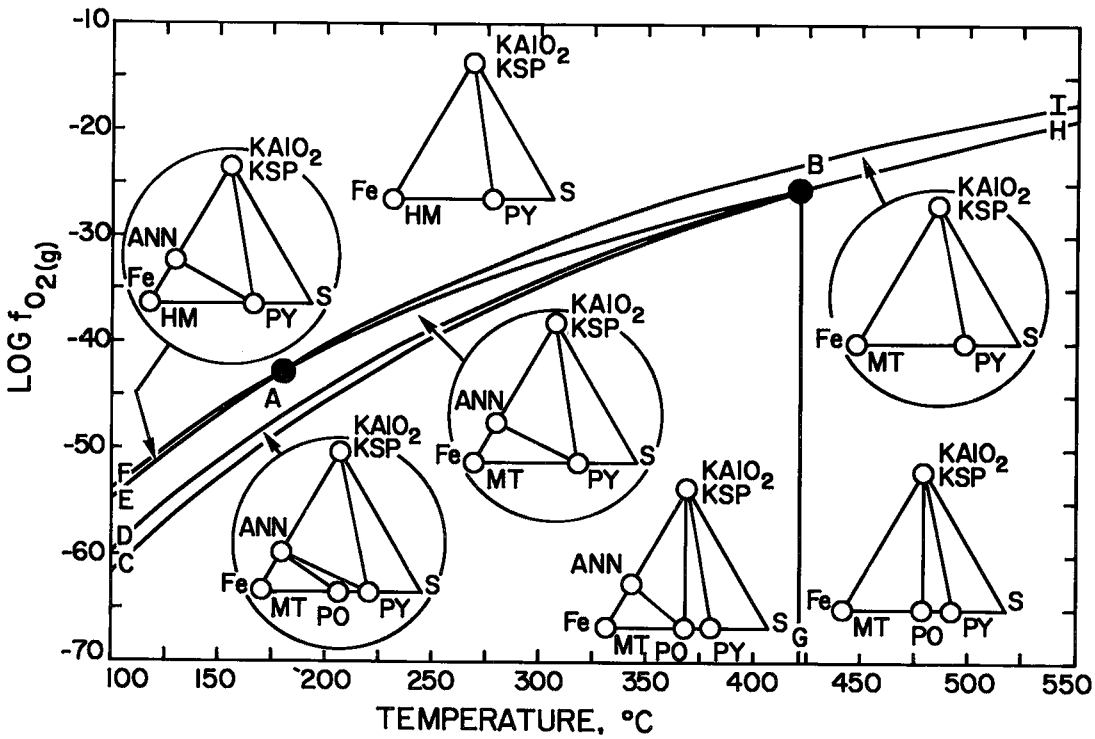

FIG. 2. Logarithm of the fugacity of oxygen gas ($f_{O_2(g)}$) buffered by the equilibrium mineral assemblages depicted in the triangular phase-diagrams as a function of temperature along the fluid pressure profile shown in Figure 4. The reactions represented by the univariant curves and invariant points (filled circles) are listed in Table 1, and the mineral abbreviations are identified in Figure 13.

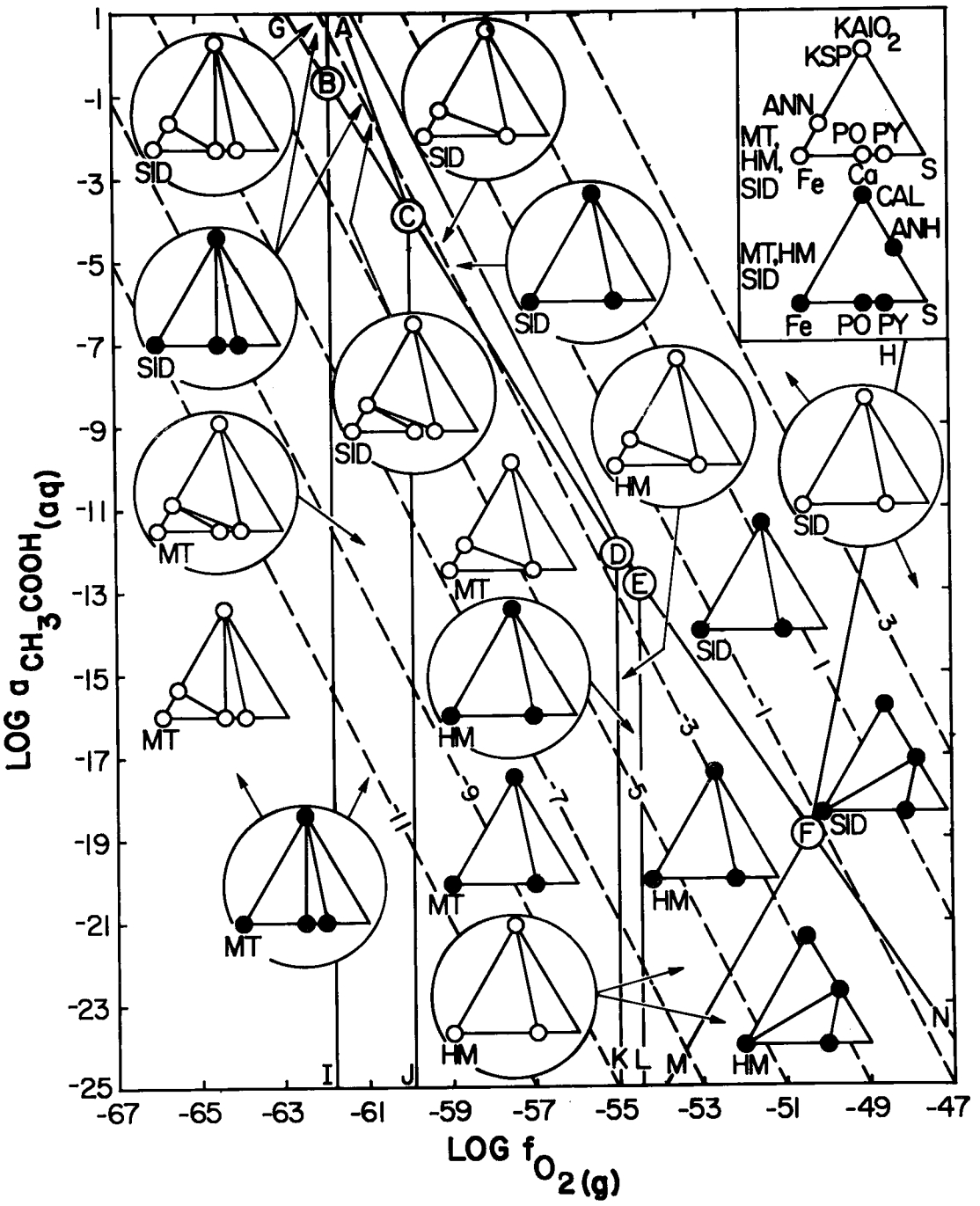

FIG. 3. Logarithm of the activity of acetic acid in an aqueous phase ($a_{CH_3COOH(aq)}$) coexisting with quartz, calcite, and the mineral assemblages depicted in the triangular phase-diagrams for the system $KAlO_2$–SiO_2–Ca–Fe–S–O–CO_2–H_2O as a function of the logarithm of the equilibrium fugacity of oxygen ($f_{O_2(g)}$) at 100°C and 400 bars (see text). Equilibrium values of log $a_{CO_2(aq)}$ are represented by the dashed curves. The mineral abbreviations are identified in Figure 13.

TABLE 1. SUMMARY OF REACTIONS REPRESENTED BY THE UNIVARIANT CURVES AND INVARIANT POINTS SHOWN IN FIGURE 2

Univariant Curve and/or Invariant Point	Reaction
CB	$2KFe_3(AlSi_3)O_{10}(OH)_2 + 6\,FeS_2 \rightleftarrows 12\,FeS + 2KAlSi_3O_8 + 3\,O_{2(g)} + 2\,H_2O_{(l)}$ (annite) (pyrite) (pyrrhotite) (K-feldspar)
DBH	$Fe_3O_4 + 3\,FeS_2 \rightleftarrows 6\,FeS + 2\,O_{2(g)}$ (magnetite) (pyrite) (pyrrhotite)
EAI	$6\,Fe_2O_3 \rightleftarrows 4\,Fe_3O_4 + O_{2(g)}$ (hematite) (magnetite)
FA	$4\,KAlSi_3O_8 + 6\,Fe_2O_3 + 4\,H_2O_{(l)} \rightleftarrows 4KFe_3(AlSi_3)O_{10}(OH)_2 + 3\,O_{2(g)}$ (K-feldspar) (hematite) (annite)
AB	$2\,KAlSi_3O_8 + 2\,Fe_3O_4 + 2\,H_2O_{(l)} \rightleftarrows 2KFe_3(AlSi_3)O_{10}(OH)_2 + O_{2(g)}$ (K-feldspar) (magnetite) (annite)
A	$KFe_3(AlSi_3)O_{10}(OH)_2 + 3\,Fe_2O_3 \rightleftarrows KAlSi_3O_8 + 3\,Fe_3O_4 + H_2O_{(l)}$ (annite) (hematite) (K-feldspar) (magnetite)
B and BG	$4KFe_3(AlSi_3)O_{10}(OH)_2 + 3\,FeS_2 \rightleftarrows 6\,FeS + 4KAlSi_3O_8 + 3\,Fe_3O_4 + 4\,H_2O_{(l)}$ (annite) (pyrite) (pyrrhotite) (K-feldspar) (magnetite)

in the present study is based on the observation that NaCl is the predominant electrolyte in most oil-field brines and hydrothermal solutions (Helgeson 1970). Calculation and extrapolation of osmotic coefficients for NaCl solutions using equations and parameters taken from Helgeson *et al.* (1981) and Pitzer *et al.* (1984) indicate that the activity of H_2O in these solutions falls in the range $0.9 \lesssim a_{H_2O} \lesssim 1$ for ionic strengths up to ~3 at the pressures and temperatures considered in the present communication.

Equation (42) constitutes a bridge between oxidation/reduction mineral equilibria and metastable equilibria among oxidized carbon-bearing species in aqueous solutions and reduced hydrocarbon species in petroleum. For example, logarithmic analogs of the law of mass action for mineral equilibria that buffer f_{O_2} like those represented by the curves shown in Figure 2 can be combined with Eqn. (42) to generate diagrams like that shown in Figure 3, which can be regarded as an isothermal–isobaric petrogenetic grid for minerals coexisting with quartz and an aqueous phase in the system $KAlO_2$–SiO_2–Ca–Fe–S–O–CO_2–H_2O at 100°C and 300 bars. Many of the minerals shown in Figure 3 are commonly found in hydrocarbon reservoirs (Biederman 1986).

Univariant equilibria are depicted in Figures 2 and 3 as solid curves, which meet in isothermal–isobaric invariant points at A and B in Figure 2 and B, C, D, E, and F in Figure 3. The reactions corresponding to the curves and invariant points in Figure 2 are listed in Table 1, where they are labeled with the same letter designations as those shown in the figure. Stable mineral assemblages are denoted in Figures 2 and 3 by the tie lines in the triangular diagrams depicted in the divariant stability fields. Values of log $a_{CO_{2(aq)}}$ are represented in Figure 3 by the dashed isopleths. Thermodynamic calculations using analytical data reported by Kharaka *et al.* (1977) indicate that the intersection of an isopleth for log $a_{CO_{2(aq)}} \approx -2.6$ with the coordinates represented by log $a_{CH_3COOH_{(aq)}} \approx -4$ and log $f_{O_{2(g)}} \approx -59.2$ in Figure 3 is typical of the oil-field brines at ~100°C in the Houston–Galveston and Corpus Christi areas of the Texas Gulf Coast (Helgeson *et al.* 1991, H.C. Helgeson, A.M. Knox & E.L. Shock, in prep.). It can be deduced from these values and the phase relations shown in Figure 3 that the predicted equilibrium assemblage of minerals coexisting with the brines at 100°C includes quartz, K-feldspar, biotite [represented by the $KFe_3(AlSi_3)O_{10}(OH)_2$ (annite) component], siderite (or ferroan calcite or dolomite), pyrite, and calcite,

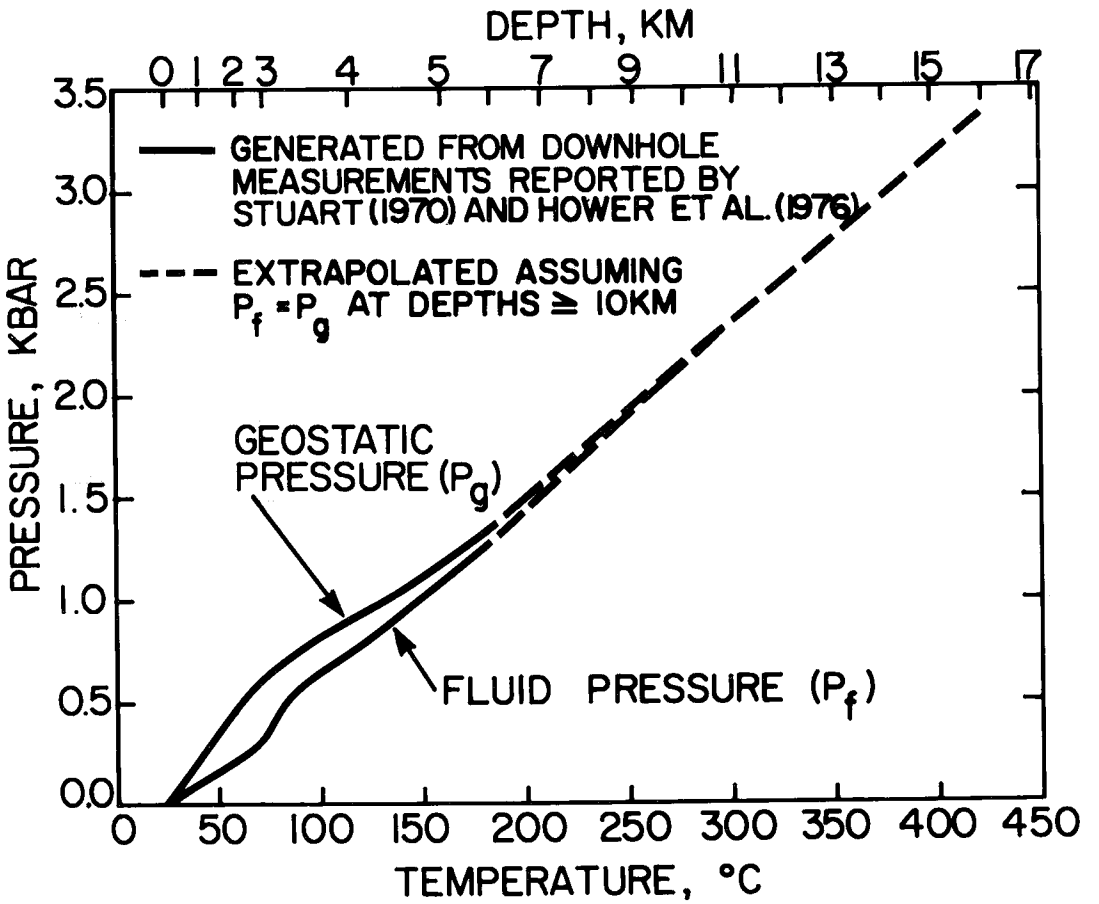

FIG. 4. Geostatic and fluid pressures as a function of depth and temperature in the Mississippi Gulf Coast. The geostatic pressure is consistent with a bulk density of 2.26 g cm^{-3}, and the profile of fluid pressure is for a fluid density equivalent to that of a brine containing 80,000 ppm NaCl (Stuart 1970).

all of which occur at depth in the Mississippi Gulf Coast (Biederman 1986, Sassen *et al.* 1989, J.J. Hanor, pers. comm., 1989). Although detrital magnetite also is present in these sediments, thermodynamic calculations indicate that this mineral is not in equilibrium with the interstitial brines, nor apparently are detrital pyrrhotite and K-feldspar, which should react with siderite to form pyrite and the annite component of biotite at the temperatures (80°–150°C) and fluid pressure (~400 bars) prevailing in the hydrocarbon reservoirs of the Houston–Galveston and Corpus Christi areas of the Texas Gulf Coast (Helgeson *et al.* 1991, H.C. Helgeson, A.M. Knox & E.L. Shock, in prep.). Similarly, detrital magnetite should react with the interstitial brines to produce siderite or pyrite (or both). Although siderite is rarely reported to be present in hydrocarbon reservoirs, it may be easily misidentified petrographically as calcite if the observer is not looking for siderite (J.R. Boles, pers. comm.).

The phase relations described above provide a framework for investigating the consequences of progressive metamorphism of hydrocarbon reservoirs and source rocks with increasing depth and temperature. To illustrate the approach, equilibrium constraints on phase relations like those shown in Figure 3 can be evaluated along a "typical" geothermal profile in a subsiding basin. The profile selected for this purpose in the present study is represented by the fluid pressure curve shown in Figure 4, which was generated from fluid pressure and temperature measurements at various depths in the Mississippi Gulf Coast reported by Stuart (1970) and Hower *et al.* (1976). The fluid pressure profile in Figure 4 was chosen instead of the geostatic profile because thermodynamic equilibrium among minerals and aqueous solutions in

nonhydrostatically stressed systems such as sedimentary basins depends at a given temperature and bulk composition solely on fluid pressure, not on overburden pressure (Bruton & Helgeson 1983, Holdaway & Goodge 1990).

Metastable equilibrium among *n*-alkane species in petroleum and coexisting oil-field waters along the fluid pressure profile shown in Figure 4 can be described in terms of the general reaction

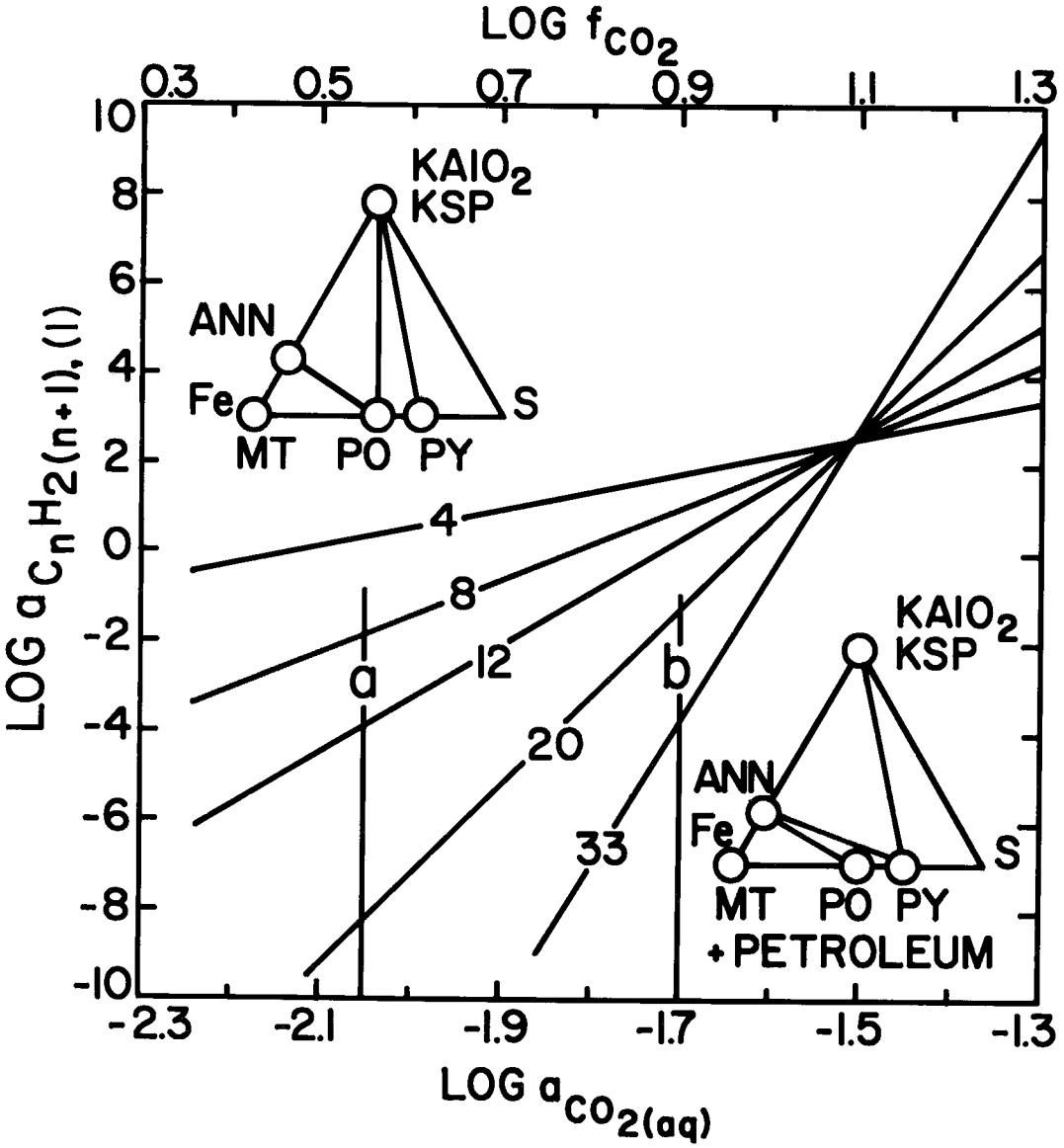

FIG. 5. Logarithms of the activities of *n*-alkanes in crude oil ($a_{C_nH_{2(n+1)},(l)}$) as a function of the logarithm of the activity of aqueous CO_2 ($a_{CO_{2(aq)}}$) in metastable equilibrium with *n*-alkanes and other hydrocarbons in petroleum and the mineral assemblages depicted in the triangular phase diagrams at 200°C along the fluid pressure profile shown in Figure 4. the numbers on the curves denote the carbon numbers of the *n*-alkanes (see text). Lines *a* and *b* refer to two particular crude oils, which are similarly annotated in Figures 7 and 8. The mineral abbreviations are identified in Figure 13.

$$C_nH_{2(n+1),(l)} + \left(\frac{3n+1}{2}\right)O_{2(g)} \rightleftarrows nCO_{2(aq)} + (n+1)H_2O \quad (43)$$

where the subscript (l) denotes the liquid state, and n again stands for the carbon number of the organic species, which corresponds to the stoichiometric number of moles of carbon atoms in one mole of the organic molecule. The logarithmic analog of the law of mass action for reaction (43) can be written for $a_{H_2O} \approx 1$ (see above) as

$$\log a_{C_nH_{2(n+1),(l)}} = \log K_n + n \log a_{CO_{2(aq)}} - \left(\frac{3n+1}{2}\right) \log f_{O_{2(g)}} \quad (44)$$

where K_n stands for the equilibrium constant for the nth statement of reaction (43). Equation (44) is plotted in Figure 5 for n = 4, 8, 12, 20, and 33 in petroleum coexisting with an aqueous solution and K-feldspar, annite, pyrite, and pyrrhotite at 200°C along the fluid pressure curve shown in Figure 4. The oxygen fugacity characteristic of this assemblage corresponds to that shown for 200°C along curve CB in Figure 2, which represents the reaction with the same label in Table 1. The law of mass action for this reaction can be written for stoichiometric K-feldspar, annite, pyrite, and pyrrhotite coexisting with an aqueous solution for which $a_{H_2O} \approx 1$ (see above) as

$$\log f_{O_2} = \frac{\log K}{3} \quad (45)$$

where K refers to the equilibrium constant for reaction CB.

Equilibrium values of log $f_{CO_{2(g)}}$ are shown at the top of the diagram depicted in Figure 5. These values were computed from the law of mass action for

$$CO_{2(aq)} \rightleftarrows CO_{2(g)} \quad (46)$$

which can be written in its logarithmic form as

$$\log f_{CO_{2(g)}} = \log K + \log a_{CO_{2(aq)}} \quad (47)$$

where K stands for the equilibrium constant for reaction (46). Equation (47) is plotted in Figure 6 for 100°, 200°, 300°, and 400°C along the fluid pressure curve in Figure 4. It can be deduced from the isotherms in this figure that log $f_{CO_{2(g)}}$ for a given log $a_{CO_{2(aq)}}$ is insensitive to temperature and pressure along the fluid pressure profile shown in Figure 4, but it maximizes slightly with increasing temperature from 100° to 400°C.

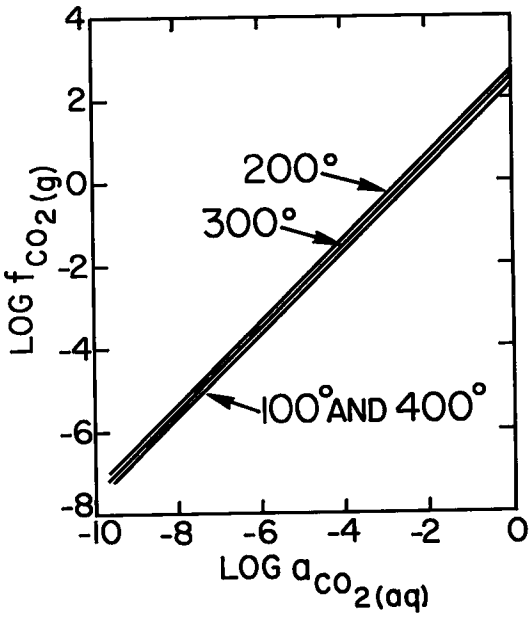

FIG. 6. Logarithm of the fugacity of CO_2 gas ($f_{CO_{2(g)}}$) as a function of the logarithm of the equilibrium activity of aqueous CO_2 ($a_{CO_{2(aq)}}$) at constant temperature (labeled in °C) along the fluid pressure profile shown in Figure 4.

The equilibrium state depicted in Figure 5 can be described in terms of the logarithmic analog of the law of mass action for

$$\underset{\text{(K-feldspar)}}{(3n+1)\,KAlSi_3O_8} + \underset{\text{(pyrrhotite)}}{6(3n+1)\,FeS} + 3n_{CO_{2(aq)}} + 2(3n+2)\,H_2O \rightleftarrows \underset{\text{(annite)}}{(3n+1)\,KFe_3AlSi_3O_{10}(OH)_2} + \underset{\text{(pyrite)}}{3(3n+1)\,FeS_2} + \underset{\text{(n-alkane)}}{3C_nH_{2(n+1),(l)}} \quad (48)$$

which can be written for $a_{KAlSi_3O_8} = a_{FeS} = a_{KFe_3(AlSi_3)O_{10}(OH)_2} = a_{H_2O} \approx 1$ as

$$\log a_{C_nH_{2(n+1),(l)}} = \log K + 3 \log a_{CO_{2(aq)}} \quad (49)$$

where K stands for the equilibrium constant for reaction (48). No attempt was made in the present study to take into account the equilibrium consequences of compositional variation in minerals on the distribution of n-alkanes in the coexisting metastable crude oil. Preliminary calculations

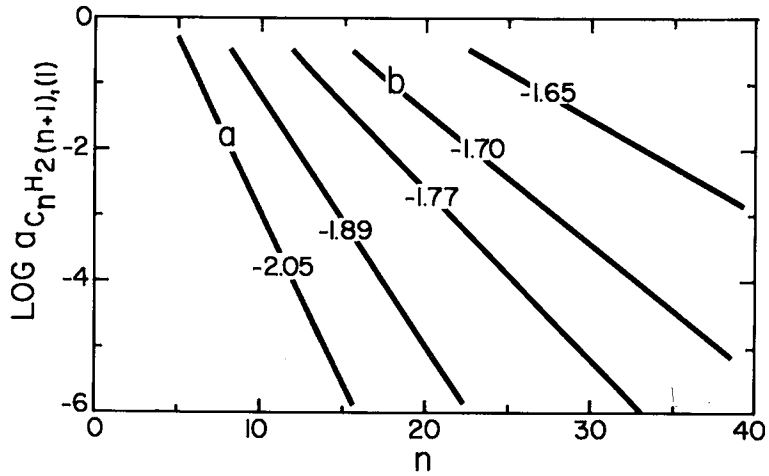

FIG. 7. Logarithm of the activities of *n*-alkanes in crude oil ($a_{C_nH_{2(n+1),(l)}}$) as a function of carbon number (n) at constant log $a_{CO_{2(aq)}}$ (represented by the numbers on the curves) at 200°C along the fluid pressure profile shown in Figure 4. The letters *a* and *b* denote particular crude oils similarly designated in Figures 5 and 8.

indicate that these effects are negligible in the present context. Reaction (48) is represented in Figure 5 by the different tie-lines in the triangular phase-diagrams on opposite sides of the bundle of *n*-alkane isopleths. It can be seen that the slopes of these isopleths decrease dramatically with decreasing carbon number, and that all of the curves intersect each other at log $a_{C_nH_{2(n+1),(l)}} = 2.3$ and log $a_{CO_{2(aq)}} = 1.51$, where log K for reaction (49) is independent of carbon number (see below).

Equilibrium speciation of n-alkanes in petroleum

The equilibrium distribution of *n*-alkanes in a

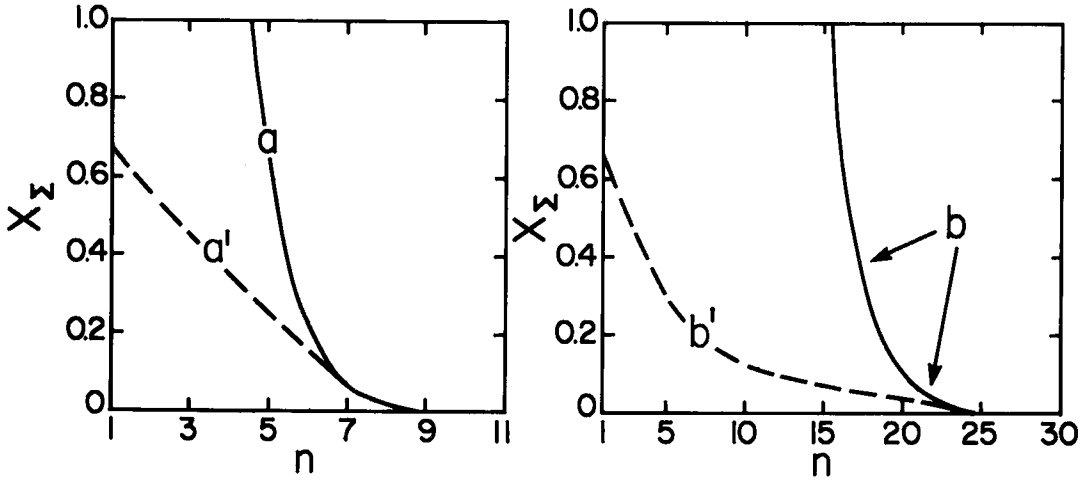

FIG. 8. Total mole fraction of *n*-alkanes (X_Σ) computed from Eqn. (50) for crude oils *a* and *b* in Figures 5 and 7 as a function of carbon number. The solid curves represent homogeneous metastable equilibrium as well as heterogeneous metastable equilibrium with aqueous CO_2, but the dashed curves annotated *a'* and *b'* designate nonequilibrium distributions of the light *n*-alkanes (see text).

given crude oil coexisting with the mineral assemblage shown in Figure 5 corresponds to a particular log $a_{CO_2(aq)}$. Two such crude oils representing typical activities of aqueous CO_2 in hydrothermal solutions are designated *a* and *b* in this figure. Log $a_{C_nH_{2(n+1),(l)}}$ for the two values of log $a_{CO_2(aq)}$ represented by *a* and *b* in Figure 5 is plotted as a function of carbon number in Figure 7, together with log $a_{C_nH_{2(n+1),(l)}}$ for crude oils represented by intermediate values of log $a_{CO_2(aq)}$. It can be seen in Figure 7 that the curves are linear, which is a consequence of the fact that log K for reaction (49) and the apparent standard partial molal Gibbs free energies of formation of *n*-alkanes (as well as other groups of organic molecules) are linear functions of carbon number. The slopes of the curves in Figure 7 are negative, and the slope increases with increasing log $a_{CO_2(aq)}$ and approaches zero at log $a_{CO_2(aq)} = -1.51$ in Figure 5. Note that the curves approach log $a_{C_nH_{2(n+1),(l)}} = 0$ at carbon numbers ranging from ~4 for curve *a* to ~13 for curve *b*. As a consequence, homogeneous equilibrium among the *n*-alkanes in crude oils *a* and *b* in Figure 7 cannot be achieved at carbon numbers lower than ~7 and ~23, respectively. This can be demonstrated with the aid of Figure 8, where the sums of the mole fractions of the *n*-alkanes in crude oils *a* and *b* are plotted against carbon number. The solid curves shown in this figure were generated from

$$X_\Sigma \equiv \sum_{i=0}^{29} X_{C_nH_{2(n+1),(l)}} \tag{50}$$

where X_Σ stands for the total mole fraction of liquid *n*-alkanes, $X_{C_nH_{2(n+1),(l)}}$ denotes the mole fraction of the subscripted species, and

$$i = 30 - n. \tag{51}$$

The values of $X_{C_nH_{2(n+1),(l)}}$ corresponding to the curves annotated *a* and *b* in Figure 8, which represent homogeneous equilibrium, were generated from Eqn. (50) using the values of $a_{C_nH_{2(n+1),(l)}}$ corresponding to curves *a* and *b* in Figure 7, respectively, and the relation

$$X_{C_nH_{2(n+1),(l)}} = \frac{a_{C_nH_{2(n+1),(l)}}}{\lambda_{C_nH_{2(n+1),(l)}}} \tag{52}$$

where $\lambda_{C_nH_{2(n+1),(l)}}$ stands for the rational activity coefficient of the subscripted species in crude oil. The values of $\lambda_{C_nH_{2(n+1),(l)}}$ used to generate curves *a* and *b* in Figure 8 correspond to trace activity coefficients ($\lambda_{tr,C_nH_{2(n+1),(l)}}$) generated in the manner described below.

Although activity coefficients of hydrocarbons in binary and, in some instances, ternary and more complex hydrocarbon liquids can be computed from equations of state such as those developed by Cunningham (1974), Peng & Robinson (1976), Schreiber & Pitzer (1989), Anderko & Pitzer (1991),

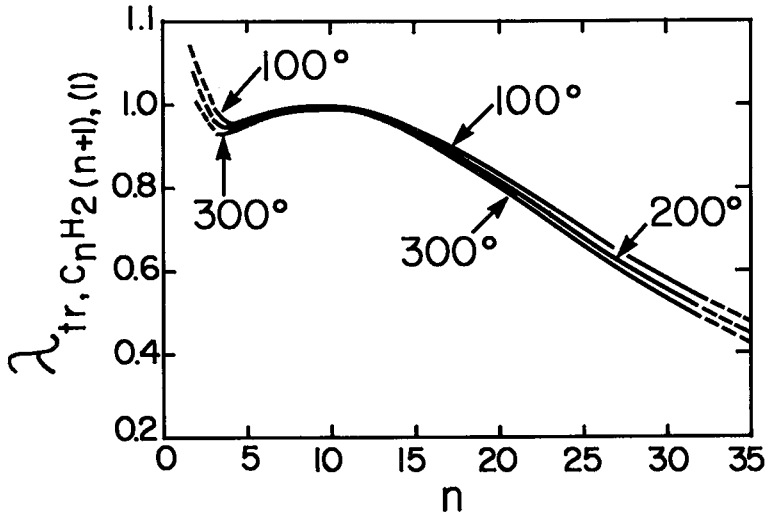

FIG. 9. Trace activity coefficients of *n*-alkanes in a model crude oil computed from the MOSCED equation developed by Thomas & Eckert (1984) for 100°, 200°, and 300°C (see text).

and others (see Prausnitz *et al.* 1986), insufficient experimental data are available for multicomponent hydrocarbon liquids at high pressures and temperatures to permit retrieval by regression calculations of appropriate mixing parameters for crude oil at depth along the fluid pressure profile in Figure 4. An alternative approach involves calculation of trace activity coefficients for species present in relatively low concentrations in crude oil ($\lambda_{tr,C_nH_{2(n+1)},(l)}$), which consists predominantly of

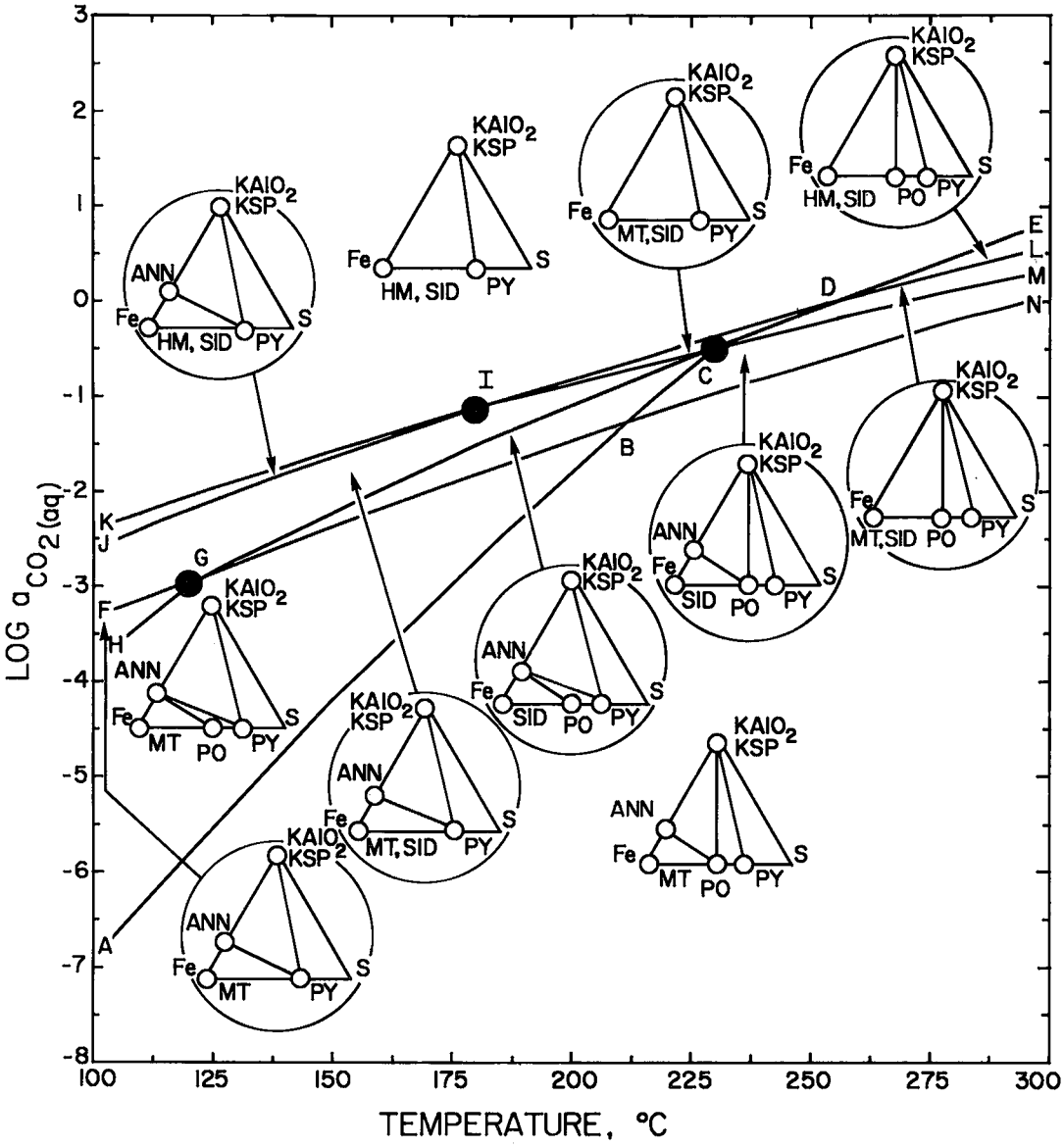

FIG. 10. Logarithm of the activity of aqueous CO_2 ($a_{CO_{2(aq)}}$) as a function of temperature for stable and metastable equilibrium among quartz, calcite, oxidized species of carbon in the aqueous phase, *n*-alkanes and other hydrocarbons in petroleum, and the mineral assemblages depicted in the triangular phase-diagrams along the fluid pressure profile shown in Figure 4. The reactions represented by the univariant curves and invariant points (filled circles) are listed in Table 2, and the mineral abbreviations are identified in Figure 13. Points B and D denote indifferent crossings of univariant curves ABC and GBN, and IDL and CDE, respectively.

light paraffins with carbon numbers less than or approximately equal to 15 (Helgeson 1991). Taking account of compositional data reported by Mair (1964) and Bestougeff (1967), a speciation model of crude oil was generated to represent the "solvent" for the various hydrocarbon species considered in the present study. Calculation of trace activity coefficients for *n*-alkanes in this model crude oil at temperatures from 100° to 300°C using the modified separation of cohesive energy density (MOSCED) equation developed by Thomas & Eckert (1984) resulted in the curves shown in Figure 9, where it can be seen that $\lambda_{tr,C_nH_{2(n+1)},(l)}$ for *n*-alkanes differs only slightly from unity for *n* less than or approximately equal to 12, but it then decreases with increasing carbon number from 0.98 at $n = 12$ to ~ 0.45 at $n = 35$. Values of $\lambda_{tr,C_nH_{2(n+1)},(l)}$ computed in this manner were used to generate the values of X_Σ shown in Figure 8 from those of $a_{C_nH_{2(n+1)},(l)}$ along curves *a* and *b* in Figure 7.

Thermodynamic consideration of the relative volume percents of *n*-alkanes and other hydrocarbons reported to be in crude oil samples subjected to analytical procedures in the laboratory indicate that the hydrocarbons in the API Research Project 6 samples for which analyses are reported by Mair (1964) may be in homogeneous metastable equilibrium with one another at temperatures below ~ 150°C, but only at fugacities of oxygen greater than those corresponding to the hematite–magnetite f_{O_2} buffer shown in Figure 2 (Helgeson 1991). It thus appears that hydrocarbon speciation in petroleum detected in the laboratory may not be representative of hydrocarbon speciation in undisturbed petroleum in hydrocarbon reservoirs. Nevertheless, extrapolation to lower carbon numbers of Mair's (1964) data for *n*-alkanes at $n \geq 10$ to compensate for the loss of the light volatile paraffins prior to collection of the API Research Project 6 samples suggests that the total number of moles of hydrocarbon species in crude oil is of the order of 7 moles liter^{-1} (Helgeson 1991). Computed mole fractions of *n*-alkanes using this value, together with analytical data taken from Mair (1964) and the extrapolated values of the number of moles liter^{-1} of *n*-alkanes in the API Research Project 6 samples at $n > 10$ resulted in the dashed curves labeled a′ and b′ in Figure 8. These curves represent two of many possible nonequilibrium distributions of *n*-alkanes in the lighter paraffin range of crude oils a′a and b′b in Figure 8. At carbon numbers higher than ~ 7 and ~ 23, respectively, all of the *n*-alkanes in crude oils *a* and *b* may be in homogeneous metastable equilibrium with each other, as well as in heterogeneous metastable equilibrium with the mineral assemblage and coexisting aqueous solutions represented by the curves shown in Figure 5. However, metastable equilibrium cannot be achieved among both light and heavy *n*-alkanes in petroleum (Helgeson 1991). Regardless of the temperature and pressure, the relative characteristics of the curves shown in Figures 5, 7, and 8 are typical of those for other mineral assemblages in metastable equilibrium with *n*-alkanes in crude oil. In all cases, the identities of the predominant *n*-alkanes in homogeneous metastable equilibrium with one another in petroleum are sensitive functions of log $a_{CO_{2(aq)}}$, but the reverse is not true (see below).

Stable and Metastable Phase Relations among Minerals, *n*-Alkanes in Petroleum, and Aqueous Species in the System $KAlO_2$–SiO_2–CaO–FeO–H_2S–O–CO_2–H_2O

Stable and (in the case of reactions involving hydrocarbons) metastable phase relations among minerals, *n*-alkanes in petroleum, and oxidized aqueous carbon species are depicted in Figure 10 for $a_{C_8H_{18},(l)} = 1$ (see below) in terms of log $a_{CO_{2(aq)}}$ as a function of temperature along the fluid pressure curve shown in Figure 4. The univariant curves and invariant points shown in this figure were generated from statements of the law of mass action for the reactions listed in Table 2. The stable mineral assemblages in the divariant fields between the univariant curves include quartz and calcite coexisting with those represented by the tie lines in the triangular composition-diagrams shown in the figure. The univariant curves and invariant points in Figure 10 represent reactions with the same letter designations as those in Table 2. It can be seen in this table that two of the three invariant reactions involve *n*-alkanes that are in metastable equilibrium with mineral assemblages and aqueous species along curves HG, FG, ABC, and GCDE in Figure 10. Because the positions of these curves are relatively insensitive to hydrocarbon speciation, petroleum was represented in the calculations by *n*-octane, which was assigned a reference activity of unity. The consequences of departures of $a_{C_8H_{18},(l)}$ from this reference value are discussed below.

Reactions HG, FG, ABC, and GCDE in Table 2 represent four of nine possible metastable equilibria involving *n*-alkanes in petroleum coexisting with aqueous fluids and quartz together with other minerals in the system $KAlO_2$–SiO_2–CaO–FeO–H_2S–O–CO_2–H_2O. The other equilibria are unstable. The five reactions representing these unstable equilibria can be written as

TABLE 2. SUMMARY OF REACTIONS REPRESENTED BY THE UNIVARIANT CURVES AND INVARIANT POINTS SHOWN IN FIGURE 10

Univariant Curve and/or Invariant Point	Reaction
ABC	$3\ C_nH_{2(n+1),(l)} + (3n+1)\ KFe_3(AlSi_3)O_{10}(OH)_2 + 3(3n+1)\ FeS_2 \rightleftarrows (3n+1)\ KAlSi_3O_8 + 6(3n+1)\ FeS + 3n\ CO_{2(aq)} + 2(3n+2)H_2O_{(l)}$ (n–alkane) (annite) (pyrite) (K–feldspar) (pyrrhotite)
HG	$2\ C_nH_{2(n+1),(l)} + ((3n+1)/2)\ Fe_3O_4 + 3((3n+1)/2)\ FeS_2 \rightleftarrows 3(3n+1)\ FeS + 2n\ CO_{2(aq)} + 2(n+1)H_2O$ (n–alkane) (magnetite) (pyrite) (pyrrhotite)
FG	$3(3n+1)\ FeCO_3 + (n+1)\ H_2O \rightleftarrows C_nH_{2(n+1),(l)}\ 3(3n+1)\ Fe_3O_4 + (8n+3)\ CO_{2(aq)}$ (siderite) (n–alkane) (magnetite)
GCDE	$C_nH_{2(n+1),(l)} + (3n+1)\ FeS_2 + (3n+1)\ FeCO_3 \rightleftarrows 2(3n+1)\ FeS + (4n+1)\ CO_{2(aq)} + (n+1)H_2O$ (n–alkane) (pyrite) (siderite) (pyrrhotite)
GBN	$FeS_2 + 4\ FeCO_3 \rightleftarrows 2\ FeS + Fe_3O_4 + 4\ CO_{2(aq)}$ (pyrite) (siderite) (pyrrhotite) (magnetite)
JIDL	$FeCO_3 + Fe_2O_3 \rightleftarrows + Fe_3O_4 + CO_{2(aq)}$ (siderite) (hematite) (magnetite)
KICM	$KAlSi_3O_8 + 3\ FeCO_3 + H_2O \rightleftarrows KFe_3(AlSi_3)O_{10}(OH)_2 + 3\ CO_{2(aq)}$ (K–feldspar) (siderite) (annite)
G	$4\ C_nH_{2(n+1),(l)} + (4n+1)\ Fe_3O_4 + (8n+3)FeS_2 \rightleftarrows 4n\ FeCO_3 + 2(8n+3)\ FeS + 4(n+1)\ H_2O$ (n–alkane) (magnetite) (pyrite) (siderite) (pyrrhotite)
I	$KAlSi_3O_8 + 3\ Fe_3O_4 + H_2O \rightleftarrows KFe_3(AlSi_3)O_{10}(OH)_2 + 3\ Fe_2O_3$ (K–feldspar) (magnetite) (annite) (hematite)
C	$3\ C_nH_{2(n+1),(l)} + (4n+1)\ KFe_3(AlSi_3)O_{10}(OH)_2 + 3(3n+1)\ FeS_2 \rightleftarrows (4n+1)\ KAlSi_3O_8 + 6(3n+1)\ FeS + 3n\ FeCO_3 + (7n+4)H_2O$ (n–alkane) (annite) (pyrite) (K–feldspar) (pyrrhotite) (siderite)

$$C_nH_{2(n+1),(l)} + 3(3n+1)\,Fe_2O_3 \rightleftarrows 2(3n+1)Fe_3O_4 + nCO_{2(aq)} + (n+1)H_2O \quad (53)$$

(n-alkane) (hematite) (magnetite)

$$3C_nH_{2(n+1),(l)} + 2(3n+1)KAlSi_3O_8 + 3(3n+1)Fe_2O_3 + (3n-1)H_2O \rightleftarrows 2(3n+1)KFe_3(AlSi_3)O_{10}(OH)_2 + 3nCO_{2(aq)} \quad (54)$$

(n-alkane) (K-feldspar) (hematite) (annite)

$$C_nH_{2(n+1),(l)} + (3n+1)KAlSi_3O_8 + (3n+1)Fe_3O_4 + 2nH_2O \rightleftarrows (3n+1)KFe_3(AlSi_3)O_{10}(OH)_2 + nCO_{2(aq)} \quad (55)$$

(n-alkane) (K-feldspar) (magnetite) (annite)

$$2(3n+1)FeCO_3 + (n+1)H_2O \rightleftarrows C_nH_{2(n+1),(l)} + (3n+1)\,Fe_2O_3 + (5n+2)CO_{2(aq)} \quad (56)$$

(siderite) (n-alkane) (hematite)

and

$$(3n+1)CaCO_3 + (3n+1)FeS_2 + (3n+1)H_2O \rightleftarrows 3C_nH_{2(n+1),(l)} + (3n+1)CaSO_4 + (3n+1)FeS + CO_{2(aq)}. \quad (57)$$

(calcite) (pyrite) (n-alkane) (anhydrite) (pyrrhotite)

The phase assemblage represented by reaction (53) is unstable because the equilibrium constant for the reaction requires the activity of aqueous CO_2 to be higher at all temperatures than the upper stability-limit of magnetite in Figure 10. Similarly, in the case of the metastable equilibrium-states represented by reactions (54) and (55), $a_{CO_{2(aq)}}$ must be higher at all temperatures than the upper stability-limit of annite and annite + magnetite, respectively. Hence, these equilibria also are unstable. Reaction (56) represents an unstable phase-assemblage because its equilibrium constant requires an activity of aqueous CO_2 at all temperatures that is below the lower limits of hematite stability. Finally, the phase assemblage represented by reaction (57) is unstable because it can occur only at activities of $CO_{2(aq)}$ that are far below the stability field of anhydrite.

It follows from the observations summarized in the preceding paragraph that the presence of crude oil in which n-alkanes are in metastable equilibrium with aqueous CO_2 in hydrocarbon reservoirs and source rocks favors the irreversible reaction of n-alkanes and detrital hematite to form authigenic magnetite and $CO_{2(aq)}$ until all of the hematite is destroyed. Similarly, $C_nH_{2(n+1),(l)}$ should react irreversibly with K-feldspar and hematite or K-feldspar and magnetite to produce iron-rich biotite and $CO_{2(aq)}$. Also, detrital hematite should react with n-alkanes and $CO_{2(aq)}$ to form siderite, *and* $C_nH_{2(n+1),(l)}$ *should react irreversibly with anhydrite, pyrrhotite, and* $CO_{2(aq)}$ *to produce pyrite and calcite until all of the anhydrite or petroleum is consumed.* The latter observation is particularly relevant to hydrocarbon accumulations associated with the cap rocks of salt domes.

It can be seen in Figure 10 that log $a_{CO_{2(aq)}}$ increases with increasing temperature along each of the univariant curves shown in the figure, all but one of which (AB) are within ~1 log unit of each other at any given temperature. Of the reactions involving n-alkanes, those labeled HG and FG in Table 2 terminate in Figure 10 at invariant point G, which occurs at 120°C along the fluid pressure profile depicted in Figure 4. At higher temperatures, only pyrrhotite, siderite, and pyrite or K-feldspar, biotite, pyrrhotite, and pyrite can coexist in metastable equilibrium with aqueous CO_2 and n-alkanes in petroleum. The latter of these two metastable equilibria is represented by curve ABC in Figure 10, which terminates at invariant point C. Point B in this figure designates an indifferent crossing of univariant curves ABC and GBN. At temperatures above invariant point C, which occurs at 230°C, only one mineral assemblage in the system $KAlO_2$–SiO_2–CaO–FeO–H_2S–O–CO_2–H_2O can coexist in metastable equilibrium with aqueous CO_2 and n-alkanes in petroleum. This state of metastable equilibrium corresponds to the reversible reaction of pyrrhotite with aqueous CO_2 to form pyrite, siderite, and n-alkanes in the presence of quartz and calcite along curve GCDE in Figure

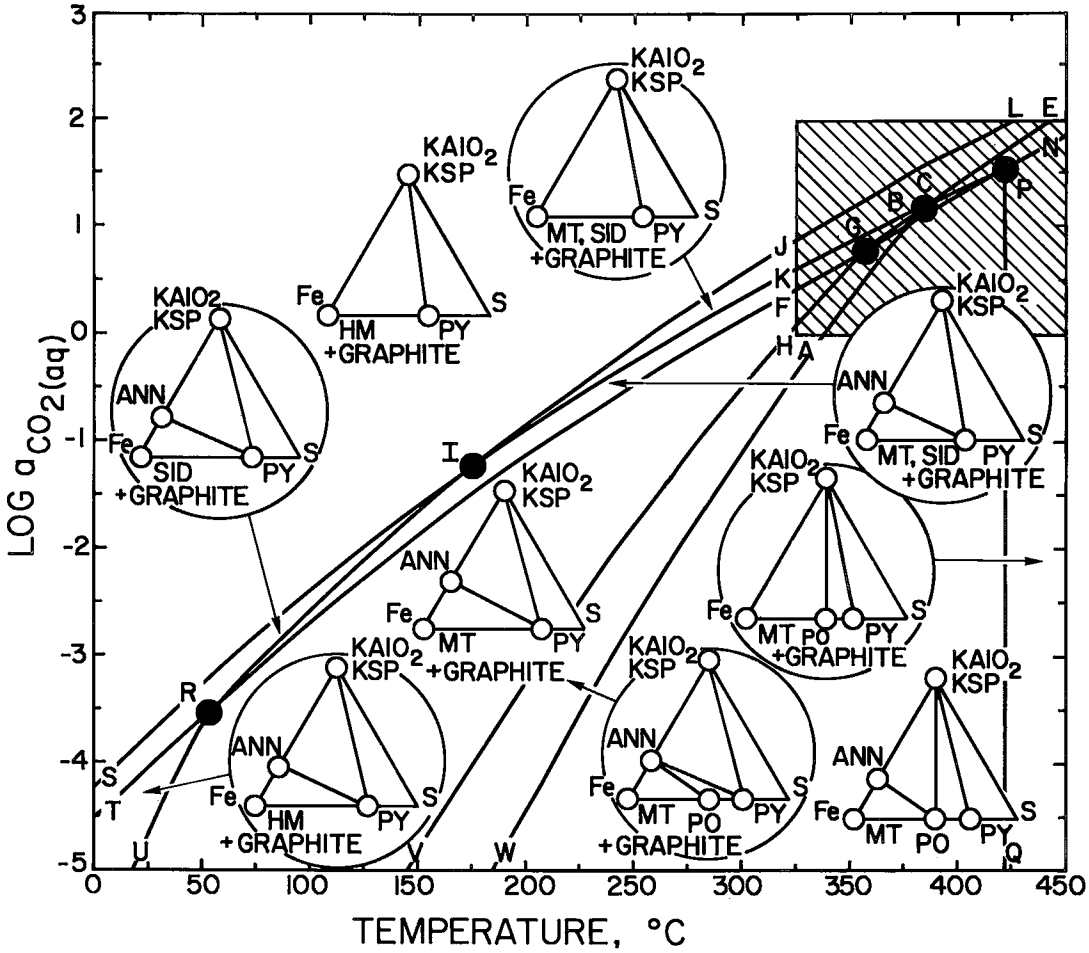

FIG. 11. Logarithm of the activity of aqueous CO_2 ($a_{CO_{2(aq)}}$) as a function of temperature for stable equilibrium among quartz, calcite, oxidized species of carbon in the aqueous phase, and the mineral assemblages depicted in the triangular phase diagrams along the fluid pressure profile shown in Figure 4. The reactions represented by the univariant curves and invariant points (filled circles) are listed in Table 3, and the mineral abbreviations are indentified in Figure 13. Point B denotes an indifferent crossing of univariant curves ABC and BN. The shaded region of the diagram is enlarged in Figure 12.

10. Point D in this figure represents an indifferent crossing of univariant curves IDL and CDE.

The metastable phase-relations depicted in Figure 10 can be compared with their stable counterparts in Figures 11 and 12, where stability relations are depicted in terms of log $a_{CO_{2(aq)}}$ and temperature for graphite coexisting with quartz, calcite, and other stable minerals in the system $KAlO_2$-SiO_2-CaO-FeO-H_2S-O-CO_2-H_2O. The univariant curves and invariant points shown in Figures 11 and 12 were generated by taking account of the law of mass action for the reactions shown in Table 3. These reactions are designated by letters corresponding to those denoting the curves and invariant points in Figures 11 and 12. All of the latter designations for both stable and metastable equilibria shown in Table 2 and Figure 10 are the same as those denoting the corresponding stable equilibria in Table 3 and Figures 11 and 12.

It can be deduced from comparison of Figure 10 with Figures 11 and 12 that metastable equilibrium among minerals, aqueous CO_2, and *n*-alkanes in petroleum causes invariant points G and C to occur at much lower temperatures (by ~240° and ~150°C, respectively) in Figure 10 than their stable counterparts for corresponding equilibria involving graphite in Figures 11 and 12. Invariant point P and curve PQ in Figures 11 and 12 correspond to

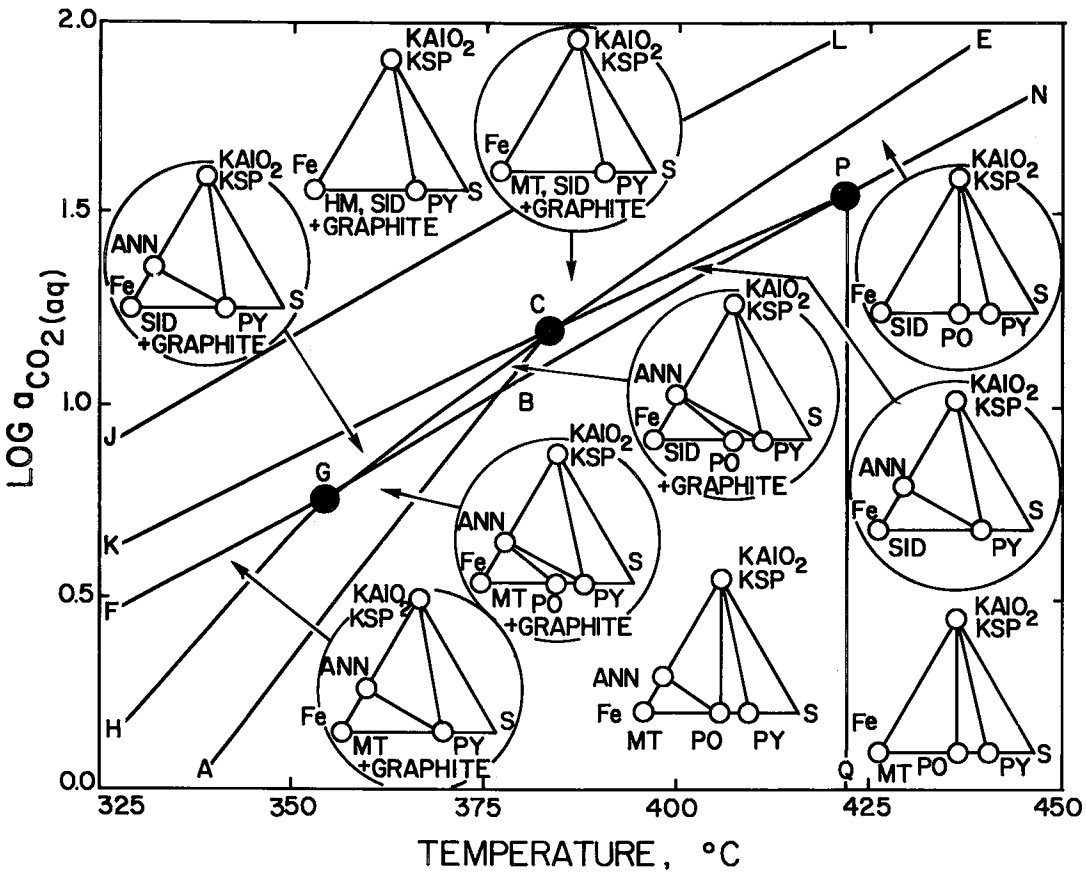

FIG. 12. Logarithm of the activity of aqueous CO_2 ($a_{CO_{2(aq)}}$) as a function of temperature in the shaded region of Figure 11, depicting stable equilibrium among quartz, calcite, oxidized species of carbon in the aqueous phase, and the mineral assemblages depicted in the triangular phase diagrams along the fluid pressure profile shown in Figure 4 (see caption of Fig. 11).

invariant point B and curve BC in Figure 2. These curves and invariant points represent the upper-temperature stability limit of annite along the fluid pressure profile shown in Figure 4.

Although the phase relations involving hydrocarbons depicted in Figure 10 are metastable relative to those depicted in Figures 11 and 12, they may nevertheless persist over long periods of geological time. Ample evidence indicates that this is the case in hydrocarbon reservoirs and source rocks, as well as hydrocarbon-bearing rocks that have been sampled at temperatures as high as 300°C (Price 1982, 1983, 1991, Price *et al.* 1979, 1981, 1986). The extent to which metastable phase-relations involving hydrocarbons like those shown in Figure 10 persist in geological systems during metamorphism can also be assessed with the aid of isotopic studies and fluid-inclusion analyses from metamorphosed source-rocks and reservoirs (see below).

As indicated above, curves HG, FG, ABC, and GCDE in Figure 10 were generated for $a_{C_8H_{18,(l)}} = 1$. Although the specification of *n*-alkanes in metastable equilibrium with aqueous CO_2 is highly sensitive to the magnitude of $a_{CO_{2(aq)}}$, the sensitivity of log $a_{C_nH_{2(n+1),(l)}}$ to log $a_{CO_{2(aq)}}$ is greater for reactions involving siderite than it is for reactions HG and ABC. Metastable equilibrium among $CO_{2(aq)}$ and *n*-alkane species in petroleum coexisting with siderite-bearing mineral assemblages along curves FG and GCDE in Figure 10 constrains log $a_{CO_{2(aq)}}$ to be within ± 0.05 or less of the values represented by the curves. In contrast, metastable equilibrium in the case of curves HG and ABC may cause log $a_{CO_{2(aq)}}$ to vary by as much as ± ~0.3 log units from the values represented by the curves, depending on the predominant *n*-alkane species in the hydrocarbon phase. Nevertheless, in all four cases, log $a_{CO_{2(aq)}}$ is sufficiently insensitive to

TABLE 3. SUMMARY OF REACTIONS REPRESENTED BY THE UNIVARIANT CURVES AND INVARIANT POINTS SHOWN IN FIGURES 11 and 12

Univariant Curve and/or Invariant Point	Reaction
SIKP	$KAlSi_3O_8 + 3\,FeCO_3 + H_2O \rightleftarrows KFe_3(AlSi_3)O_{10}(OH)_2 + 3\,CO_{2(aq)}$ (K–feldspar) (siderite) (annite)
TR	$4\,FeCO_3 \rightleftarrows 2\,Fe_2O_3 + C + 3\,CO_{2(aq)}$ (siderite) (hematite) (graphite)
UR	$6\,Fe_2O_3 + C \rightleftarrows 4\,Fe_3O_4 + CO_{2(aq)}$ (hematite) (graphite) (magnetite)
RIJL	$FeCO_3 + Fe_2O_3 \rightleftarrows + Fe_3O_4 + CO_{2(aq)}$ (siderite) (hematite) (magnetite)
RFG	$6\,FeCO_3 \rightleftarrows 2\,Fe_3O_4 + C + 5\,CO_{2(aq)}$ (siderite) (magnetite) (graphite)
VHG	$3\,FeS_2 + Fe_3O_4 + 2C \rightleftarrows 6\,FeS + 2\,CO_{2(aq)}$ (pyrite) (magnetite) (graphite) (pyrrhotite)
WABC	$2\,KFe_3(AlSi_3)O_{10}(OH)_2 + 6\,FeS_2 + 3C \rightleftarrows 2\,KAlSi_3O_8 + 12\,FeS + 3\,CO_{2(aq)} + 2\,H_2O$ (annite) (pyrite) (graphite) (K–feldspar) (pyrrhotite)
GCE	$2\,FeS_2 + 2\,FeCO_3 + C \rightleftarrows 4\,FeS + 3\,CO_{2(aq)}$ (pyrite) (siderite) (graphite) (pyrrhotite)
GPBN	$FeS_2 + 4\,FeCO_3 \rightleftarrows 2\,FeS + Fe_3O_4 + 4\,CO_{2(aq)}$ (pyrite) (siderite) (pyrrhotite) (magnetite)
Q, QP	$4\,KAlSi_3O_8 + 6\,FeS + 4\,H_2O \rightleftarrows 4\,KFe_3(AlSi_3)O_{10}(OH)_2 + 3\,FeS_2 + 3\,Fe_3O_4$ (K–feldspar) (pyrrhotite) (annite) (pyrite) (magnetite)
R	$5\,Fe_2O_3 + C \rightleftarrows 3\,Fe_3O_4 + FeCO_3$ (hematite) (graphite) (magnetite) (siderite)
I	$KAlSi_3O_8 + 3\,Fe_3O_4 + H_2O \rightleftarrows KFe_3(AlSi_3)O_{10}(OH)_2 + 3\,Fe_2O_3$ (K–feldspar) (magnetite) (annite) (hematite)
G	$12\,FeCO_3 + 30\,FeS \rightleftarrows 9\,Fe_3O_4 + 15\,FeS_2 + 12C$ (siderite) (pyrrhotite) (magnetite) (pyrite) (graphite)
C	$KFe_3(AlSi_3)O_{10}(OH)_2 + 2\,FeS_2 + C \rightleftarrows KAlSi_3O_8 + 4\,FeS + FeCO_3 + H_2O$ (annite) (pyrite) (graphite) (K–feldspar) (pyrrhotite) (siderite)

hydrocarbon speciation that the states of metastable equilibrium represented by curves FG, HG, ABC, and GCDE in Figure 10 can be regarded as log $a_{CO_{2(aq)}}$ buffers to within limits that are of the order of magnitude of the uncertainties in the computed equilibrium-constants for the reactions at high temperatures and pressures. As indicated above, the equilibrium and nonequilibrium states represented by the curves shown in Figure 8 are typical of the crude oils in the phase assemblages represented by these univariant curves (Helgeson 1991).

The states of metastable equilibrium represented by curves HG, FG, ABC, and GCDE in Figure 10 require equilibrium fugacities of methane, ethane, propane, and other light hydrocarbons that are too large to be achieved in the Earth's crust (Helgeson 1991). For example, metastable equilibrium with methane along all four of these curves would require f_{CH_4} to be $\gtrsim 10^5$ bars. In the case of the stable equilibria portrayed in Figure 11 and 12, equilibrium with methane can be achieved in the Earth's crust along all of the curves except VH and WA below ~75° and ~175°C, respectively. The fact that the fugacities of the light paraffins required for metastable equilibrium among aqueous CO_2, *n*-alkanes in petroleum, and the mineral assemblages represented by curves HG, FG, ABC, and GCDE in Figure 10 cannot be achieved in the Earth's crust precludes metastable equilibrium among the light and heavy *n*-alkanes in crude oil, which provides a driving force for hydrocarbon maturation (Helgeson 1991). It also precludes metastable equilibrium among the light paraffins and carboxylic acids, CO_2, and other oxidized species of carbon in oil-field brines, which are apparently in equilibrium with calcite. However, the light hydrocarbons in these brines may nevertheless be in metastable equilibrium with their counterparts in crude oil (Helgeson 1991).

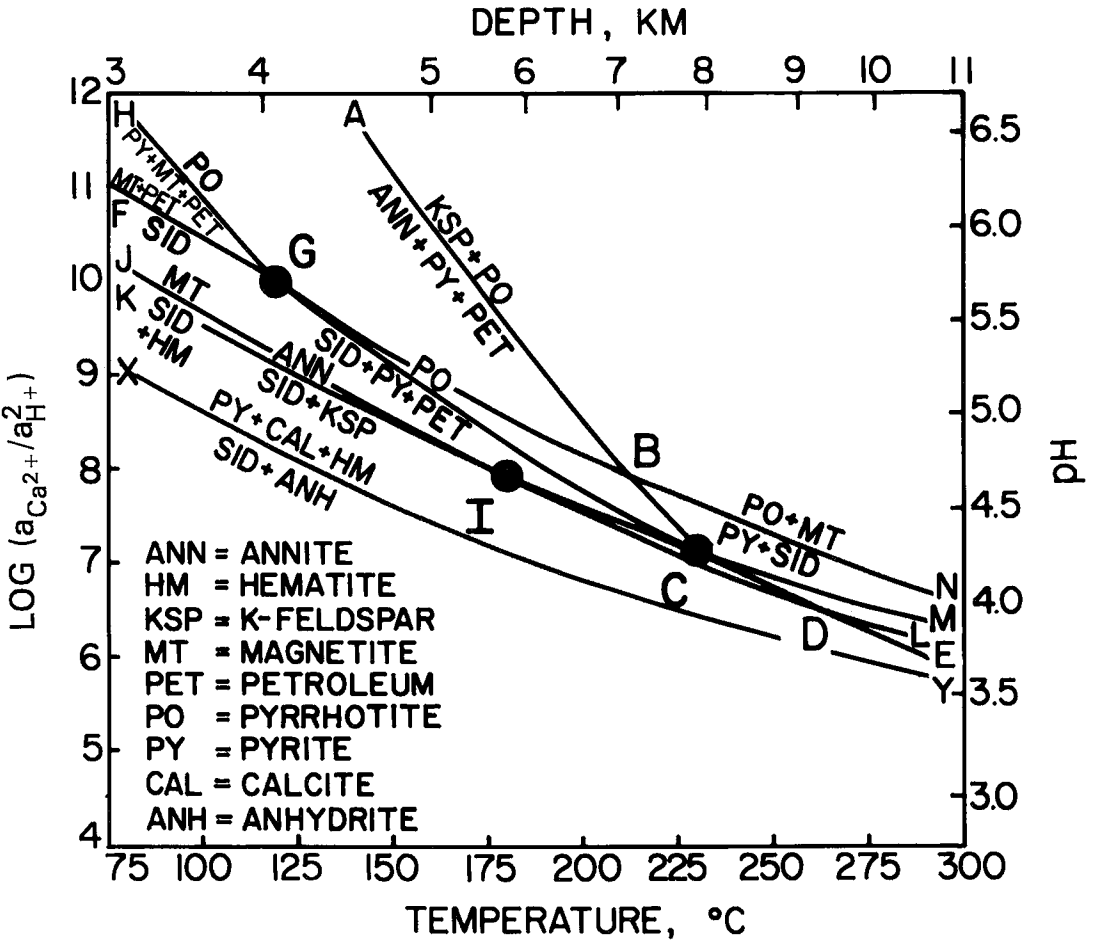

FIG. 13. Logarithm of the activity of the calcium ion over the square of the activity of the hydrogen ion (log $a_{Ca^{2+}}/a^2_{H^+}$) in aqueous solutions coexisting in stable equilibrium with quartz, calcite, and other minerals in the system $KAlO_2$–SiO_2–CaO–FeO–H_2S–O–CO_2–H_2O and (in the case of univariant curves ABC, HG, PG, and GCDE) metastable equilibrium with *n*-alkanes and other hydrocarbons in petroleum as a function of temperature along the fluid pressure profile shown in Figure 4. Points B and D denote indifferent crossings of univariant curves ABC and GBN, and IDL and CDE, respectively.

METASOMATIC CONSEQUENCES OF METASTABLE EQUILIBRIUM AMONG SILICATES, SULFIDES, OXIDES, *n*-ALKANES IN PETROLEUM, $CO_{2(aq)}$, AND COEXISTING CALCITE IN THE SYSTEM $KAlO_2$–SiO_2–FeO–CaO–H_2S–O–CO_2–H_2O

Univariant and invariant stable and (for reactions involving *n*-alkanes in petroleum) metastable equilibria in the system $KAlO_2$–SiO_2–CaO–FeO–H_2S–O–CO_2–H_2O are depicted in Figure 13 in terms of temperature and log $(a_{Ca^{2+}}/a^2_{H^+})$ in the aqueous phase along the fluid pressure profile shown in Figure 4. The labels on the curves and invariant points in Figure 13 are the same as those for the reactions listed in Table 2 and the corresponding curves and invariant points in Figure 10. The curves in Figure 13 were generated from those in Figure 10 by taking account of the law of mass action for

$$\underset{\text{(calcite)}}{CaCO_3} + 2H^+ \rightleftarrows Ca^{2+} + CO_{2(aq)} + H_2O \qquad (58)$$

which can be written in its logarithmic form for $a_{CaCO_3} = a_{H_2O} \approx 1$ (see above) as

$$\log\left(a_{Ca^{2+}} / a^2_{H^+}\right) = \log K + \log a_{CO_{2(aq)}} \qquad (59)$$

where K stands for the equilibrium constant for reaction (58). Equation (59), which is represented by the curves depicted in Figure 14, can be

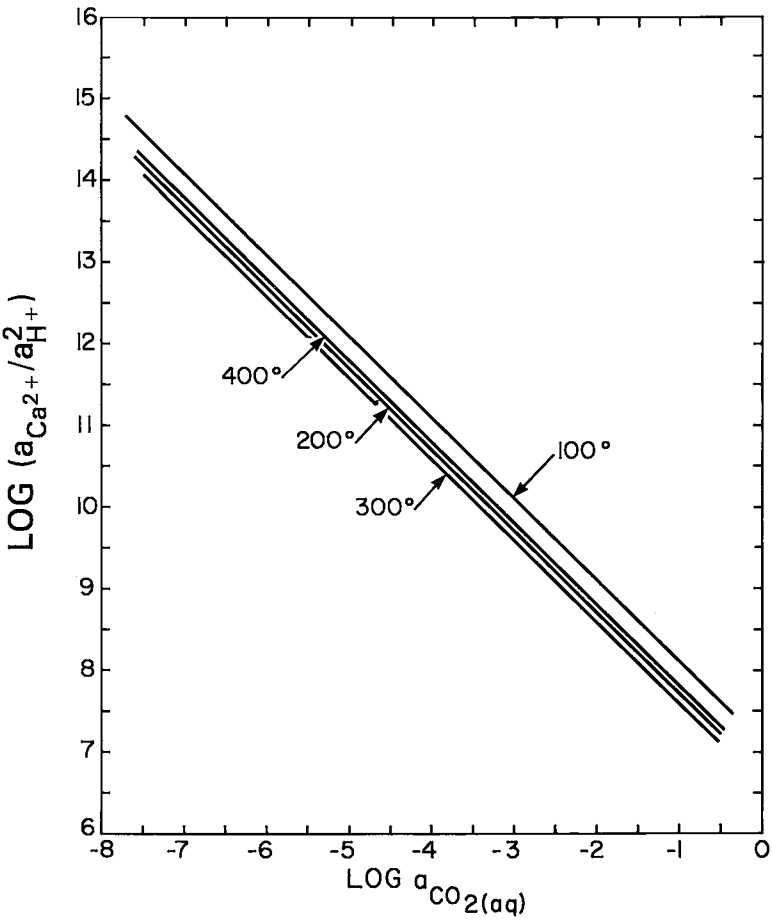

FIG. 14. Logarithm of the activity of the calcium ion over the square of the activity of the hydrogen ion (log $a_{Ca^{2+}}/a^2_{H^+}$) in an aqueous solution coexisting in stable equilibrium with calcite as a function of the logarithm of the activity of aqueous CO_2 ($a_{CO_{2(aq)}}$) at constant temperature (labeled in °C) along the fluid pressure profile shown in Figure 4.

combined with statements of the law of mass action for the reactions listed in Table 2 to generate all but one of the curves (XY) shown in Figure 13. The reaction represented by curve XY in Figure 13 can be written as

$$\underset{\text{(calcite)}}{15CaCO_3} + \underset{\text{(pyrite)}}{FeS_2} + \underset{\text{(hematite)}}{7Fe_2O_3} + 26H^+ \rightleftarrows \underset{\text{(anhydrite)}}{2CaSO_4} + \underset{\text{(siderite)}}{15FeCO_3} + 13Ca^{2+} + 13H_2O \quad (60)$$

The pH scale shown on the right side of this figure is consistent with log $a_{Ca^{2+}} = -1.4$, which was computed from the concentration of Ca^{2+} in "average" oil-field brine (3000 ppm), generated by Kinghorn (1983) using a representative value of 0.5 for the individual ion activity coefficient of Ca^{2+} in the brine. The latter value was computed from the geochemical approximation developed by Helgeson *et al.* (1981).

It can be seen in Figure 13 that the equilibrium pH shown in the figure ranges from ~6 for aqueous solutions in which CO_2 is in metastable equilibrium at 100°C with *n*-alkanes in petroleum coexisting with pyrite, pyrrhotite, and magnetite, or magnetite and siderite, to ~3.6 at 300°C for metastable equilibrium among *n*-alkanes in petroleum, Ca^{2+}, H^+, and carbonate species in the aqueous phase, and pyrrhotite, pyrite, siderite, quartz, and calcite. If the Ca^{2+} concentration in the aqueous solution were taken to be an order of magnitude higher or lower than 3000 ppm, the solution pH at a given temperature shown in Figure 13 would be half a log unit lower or higher, respectively. Changing the activity coefficient of Ca^{2+} by a few tenths has only a slight effect on the calculated values of solution pH shown in Figure 13.

It can be shown that the calculated values of pH for aqueous solutions coexisting with the various phase-assemblages represented by the univariant curves and invariant points in Figures 10 and 13 are in general agreement with independently predicted values of pH generated from equilibrium and mass-transfer calculations for a wide variety of hydrothermal systems (Helgeson 1970). Invariant point C in these figures is of particular interest in this regard because it represents equilibrium among the annite component of biotite and K-feldspar, quartz, calcite, pyrrhotite, pyrite, and siderite, all of which are in metastable equilibrium with *n*-alkanes in petroleum and oxidized species of carbon in an aqueous phase with a pH of ~4.3 at 230°C and a depth of ~8 km along the fluid pressure curve shown in Figure 4. If invariant point C is reached as a result of progressive burial of a hydrocarbon reservoir or source rock along curve ABC in Figure 13, K-feldspar, pyrrhotite, and calcite should precipitate at the expense of annite, pyrite, and *n*-alkanes, which is accompanied by an increasingly positive change in volume, resulting in decreasing porosity. If invariant point C is reached by progressive burial of a hydrocarbon source rock or reservoir along curve GC in Figure 13, pyrrhotite and calcite replace pyrite and siderite in the process, with a concomitant decrease in porosity and conversion of *n*-alkanes in petroleum to $CO_{2(aq)}$ and other oxidized aqueous species of carbon. In both cases, the reactions cause $a_{Ca^{2+}}$ and the solution pH to decrease, and $a_{CO_{2(aq)}}$ to increase, which favors replacement of detrital plagioclase by calcite. With continued burial and further reaction along curve CDE in Figures 10 and 13, the solution pH continues to decrease, and the aqueous solution becomes increasingly CO_2-rich, reaching a concentration of ~6 m (264,000 ppm) at 300°C, where the solution pH is of the order of 4 or less. The reactions accompanying progressive burial of a hydrocarbon reservoir or source rock along curves ABC or GCDE in Figures 10 and 13 also generate aqueous acetic acid in equilibrium with $CO_{2(aq)}$, but to a decreasing degree with increasing temperature (Helgeson 1991). Calculation of the activity of benzene in the hydrocarbon liquid represented by curve CDE in Figures 10 and 13 indicates that $a_{O_6H_{6,(l)}}$ increases from ~0.01 at C to ~0.1 at E. At high temperature, petroleum speciation may be dominated by aromatic hydrocarbons.

The decrease in porosity with increasing depth of burial along curves ABC and GCDE in Figure 13 favors progressive isolation of the fluids in the hydrocarbon reservoir or source rock, which promotes increasing fluid pressure toward its geostatic equivalent. Essentially all of the CO_2 in the CO_2-rich aqueous fluid at point E in Figure 13 is derived from liquid hydrocarbons during the burial process. With further burial above 300°C, all of the crude oil may be converted to CO_2, H_2O, and other species in the aqueous phase as the two fluids become completely miscible (see below). The reaction represented by curve GCDE in Figure 13 consumes H_2O. Hence, the process leads progressively to complete conversion of hydrocarbons in crude oil to carbonate in calcite and CO_2 and other oxidized species of carbon in the aqueous phase.

Temperature-X_{CO_2} Diagrams Depicting Stable and Metastable Equilibria in the System $KAlO_2$–SiO_2–CaO–FeO–H_2O–O–CO_2–H_2O

A temperature-X_{CO_2} diagram depicting stable and (in the case of curve DEE′E″) metastable equilibria in this system is depicted in Figure 15 for temperatures and depths corresponding to the fluid pressure profile shown in Figure 4. Equilibrium

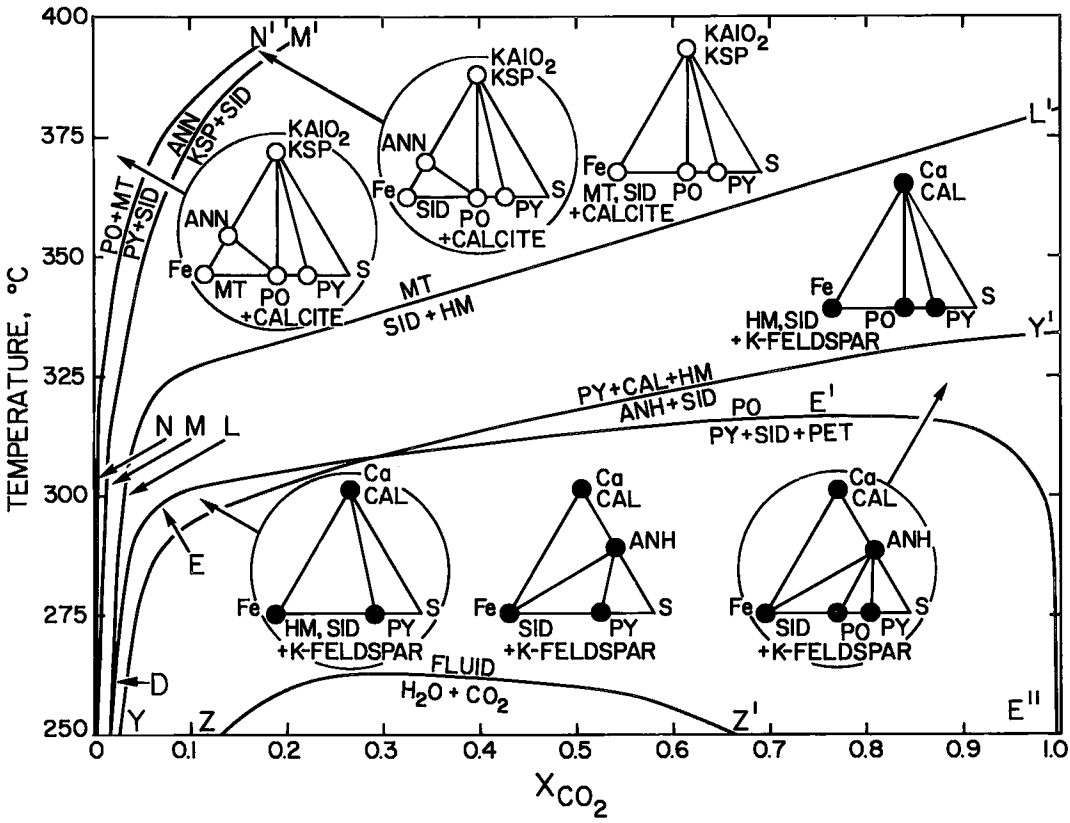

FIG. 15. Temperature–X_{CO_2} diagram representing stable and (in the case of the reaction involving *n*-alkanes in petroleum metastable equilibrium among a CO_2–H_2O fluid and quartz, calcite, and the mineral assemblages depicted in the triangular phase-diagrams for the system $KAlO_2$–SiO_2–CaO–FeO–H_2S–O–CO_2–H_2O along the fluid pressure profile shown in Figure 4. Curve DEE'E" represents metastable equilibrium among pyrrhotite, pyrite, siderite, *n*-alkanes in petroleum, and a CO_2–H_2O fluid. The letters denoting the univariant curves and invariant points (filled circles) correspond to those designating the corresponding curves and points in Figure 10 and 13. Point D represents an indifferent crossing of univariant curves IDL and CDE. The mineral abbreviations are identified in Figure 13.

among pyrite, pyrrhotite, and siderite coexisting with a CO_2–H_2O fluid in metastable equilibrium with *n*-alkanes for $n \geq 10$, as well as benzene, toluene, and other hydrocarbons in crude oil, is represented in this figure by curve DEE'E", which is an extension in T–X_{CO_2} space of curve GCDE in Figure 10. As indicated above, this is the only mineral assemblage in the system that can coexist in metastable equilibrium with hydrocarbon species in crude oil, and thereby buffer the oxygen fugacity and mole fraction of CO_2 in the system at temperatures in excess of 230°C during burial along the fluid pressure curve shown in Figure 4. The stable analog of Figure 15 is depicted in Figure 16, where stable equilibrium phase-relations are shown for graphite coexisting with a CO_2–H_2O fluid and other minerals in the system $KAlO_2$–SiO_2–CaO–FeO–H_2S–O–CO_2–H_2O. Where possible, the univariant curves and invariant points shown in Figures 15 and 16 are labeled with the same letter designations as those of the corresponding curves in Figures 10–13. The curves in Figures 15 and 16 were generated for $X_{CO_2} + X_{H_2O} \approx 1$ using the fugacity coefficients of H_2O and CO_2 shown in Figures 17 and 18, which were obtained for temperatures and pressures along the fluid pressure curve shown in Figure 4 by extrapolating fugacity coefficients computed from the modified Redlich-Kwong equation of state by Holloway (1977) and Bowers & Helgeson (1983). The curve representing the miscibility gap in the fluid in Figures 15 and 16 (curve ZZ') is consistent with the analysis by

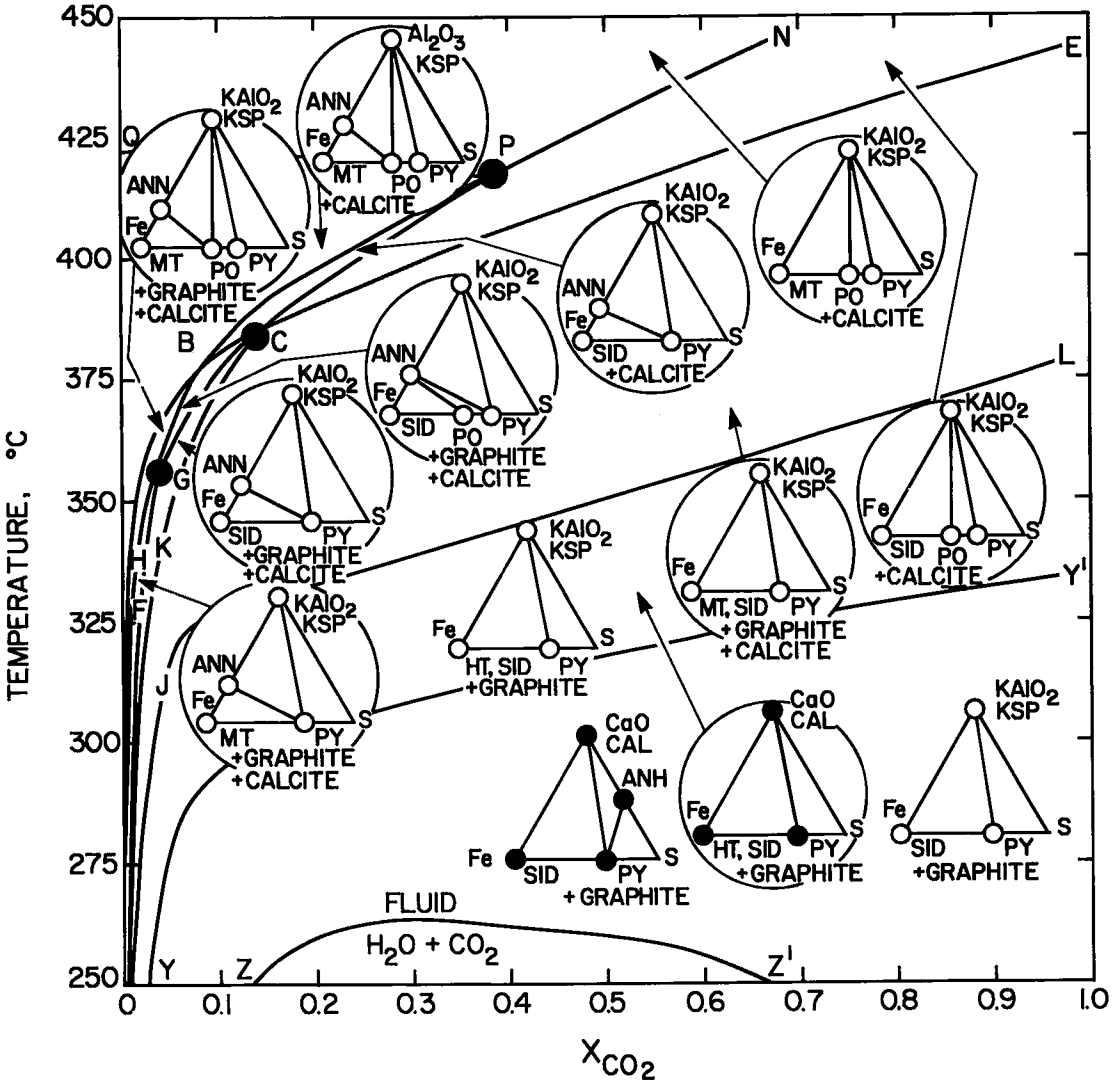

FIG. 16. Temperature-X_{CO_2} diagram representing stable equilibrium among a CO_2–H_2O fluid and quartz, calcite, and the mineral assemblages depicted in the triangular phase diagrams for the system $KAlO_2$–SiO_2–CaO–FeO–H_2S–O–CO_2–H_2O along the fluid pressure profile shown in Figure 4. Except for Z, Z′, and Y′, the letters denoting the univariant curves and invariant points (filled circles) refer to those designating reactions in Table 3 and the corresponding curves and points in Figures 11 and 12. The mineral abbreviations are identified in Figure 13. Point B represents an indifferent crossing of univariant curves ABC and GBN.

Bowers & Helgeson (1983) of phase relations in the system CO_2–H_2O.

It can be seen in Figure 15 that curve DEE′E″ reaches a maximum at ~320°C, which represents the highest temperature at which hydrocarbon species in crude oil can be in metastable equilibrium with pyrite, pyrrhotite, and siderite along the fluid pressure curve shown in Figure 4. However, it should be emphasized in this regard that 320°C is not necessarily the highest temperature at which crude oil may exist in the Earth's crust. For example, if the fugacity of oxygen in the system is not buffered by mineral assemblages coexisting in metastable equilibrium with $CO_{2(aq)}$ and hydrocarbon species in crude oil, but instead is controlled solely by metastable equilibrium among aqueous

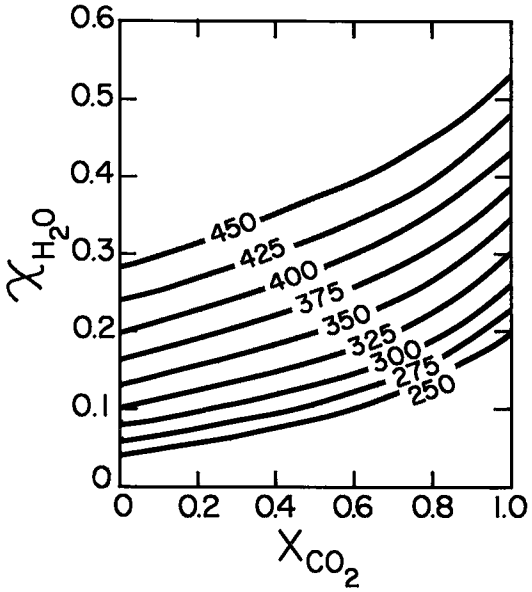

FIG. 17. Fugacity coefficient of H_2O (χ_{CO_2}) in CO_2–H_2O fluids as a function of X_{CO_2} at constant temperature (labeled in °C) along the fluid pressure profile shown in Figure 4 (see text).

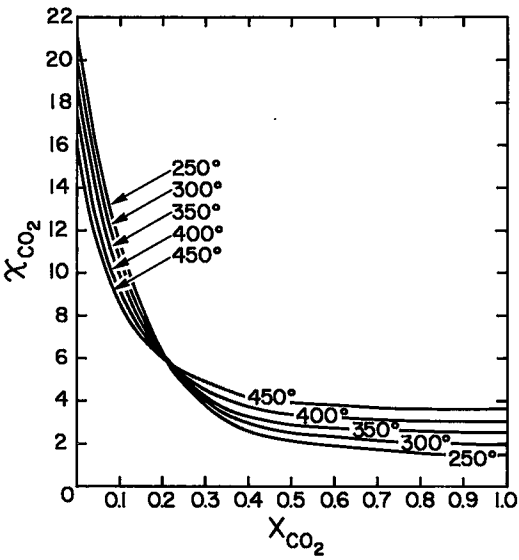

FIG. 18. Fugacity coefficient of CO_2 (χ_{CO_2}) in CO_2–H_2O fluids as a function of X_{CO_2} at constant temperature (labeled in °C) along the fluid pressure profile shown in Figure 4 (see text).

CO_2, CH_3COOH, and hydrocarbon species in petroleum, the hydrocarbon liquid may coexist with a CO_2-rich aqueous fluid at much higher temperatures than 320°C. Candidates for survival at these high temperatures include heavy aromatic-rich crude oils and asphaltenes.

Progressive burial of hydrocarbon reservoirs or source rocks along curve DEE′ in Figure 15 is accompanied by formation of pyrrhotite at the expense of siderite and pyrite as the CO_2–H_2O fluid becomes increasingly enriched in CO_2 derived from hydrocarbon species in crude oil. At point E′ in Figure 15, the mole fraction of CO_2 in the aqueous phase reaches ~0.75. With further burial and increasing temperature above ~320°C, all of the pyrite and siderite must be replaced by pyrrhotite, or all of the crude oil must be converted to CO_2. In any case, if tectonic events cause release of a CO_2-rich fluid at depths in excess of ~12 km, where the temperature exceeds ~320°C, metastable crude oil may be precipitated from the fluid as it moves in fractures toward shallower depths and lower temperatures, fluid pressures, and oxygen fugacities. As the immiscible petroleum phase precipitates, hydrocarbon species of successively higher molecular weight should form in metastable equilibrium with one another, which is the opposite order of their stoichiometric solubilities. The process favors two-phase flow, dissolution of calcite, and increasing porosity and permeability along the flow path.

CONCLUDING REMARKS

It can be deduced from the calculations described above that progressive burial of petroleum reservoirs and source rocks may lead to preservation of liquid hydrocarbons in metastable equilibrium with their mineralogical environment and $CO_{2(aq)}$, $CH_3COOH_{(aq)}$, and other oxidized aqueous species. The presence of both pyrite and pyrrhotite in the mineral assemblage is required for this state of metastable equilibrium to persist at temperatures above ~120°C. The other minerals in the assemblage may be biotite and K-feldspar, or siderite, ankerite, ferroan dolomite, or ferroan calcite. Under these conditions, petroleum with hydrocarbons in metastable equilibrium with this mineral assemblage may persist at temperatures as high as 230°C. At higher temperatures, from 230° to ~320°C, only the mineral assemblage pyrite + pyrrhotite + Fe-bearing carbonate in metastable equilibrium with hydrocarbons in petroleum and a CO_2–H_2O fluid can buffer both the fugacities of O_2 and CO_2. It follows that assemblages of pyrrhotite + pyrite + Fe-bearing carbonate in low-grade metamorphic

rocks may be associated with metastable preservation of petroleum during the metamorphism of hydrocarbon reservoirs and source rocks at temperatures and pressures of the order of 320°C and ~2.7 kbar or less. Such states of metastable equilibrium that might have been present during metamorphism should be manifested by carbon isotopes and the compositions of fluid inclusions in metasomatic minerals. The inclusions should contain aqueous carboxylic acids and other oxidized species of carbon, high concentrations of CO_2 and, in the absence of graphite, both liquid and gas hydrocarbons. The fluid inclusions also may contain abundant sulfate and possibly sulfide daughter minerals. Fluid-inclusion studies should also serve to corroborate the thermodynamic calculations summarized above, which indicate that ~320°C is the maximum temperature at which metastable equilibrium involving $CO_{2(aq)}$, hydrocarbon species in petroleum, and pyrite + pyrrhotite + Fe-bearing carbonates can be achieved during prograde metamorphism. At temperatures between 230° and 320°C, the calculations suggest that preservation of liquid hydrocarbons in metastable equilibrium with this mineral assemblage is probably limited to rocks containing ferruginous carbonates and relatively sulfur-rich crude oils. In the absence of either pyrite or pyrrhotite, heavy crude oils and asphaltenes may persist in ferruginous-carbonate-bearing rocks at temperatures in excess of 320°C. In any event, the metamorphic rocks would be expected to contain abundant sulfides in veins and veinlets throughout the paleoreservoir or source rock.

The calculations summarized above indicate that progressive burial of hydrocarbon reservoirs leads to CO_2-rich aqueous fluids at depths in excess of ~10 km. This observation, as well as the results of the thermodynamic calculations described in the preceding pages, are ripe for experimental verification. Carefully controlled experiments in which the fugacity of oxygen is buffered are needed to document the extent to which hydrocarbon species in crude oil may persist in metastable equilibrium with their mineralogical and aquatic environments at high temperatures and pressures. Other experiments are required to demonstrate that liquid hydrocarbons can indeed precipitate from CO_2-rich aqueous fluids at high temperatures and pressures. The fact that oxidized "organic" species may form at high temperatures and pressures has already been demonstrated by French (1964), who unintentionally produced propanoic acid, ethyl alcohol, butyric and acetic acids, and ketones during the synthesis of siderite in experiments at 2 kbar and temperatures from 350° to 380°C. Many more such experiments are needed to even begin to clarify the murky division between organic and inorganic reactions in metamorphic processes.

Acknowledgements

This paper could never have been written without the superb research support I have in the Laboratory of Theoretical Geochemistry (otherwise known as Prediction Central) at the University of California, Berkeley. I am indebted to Eric Oelkers for expertly and cheerfully expediting the calculations described above. Eric coded up the MOSCED equation for trace activity coefficients of organic species and the PFGC equation of state for hydrocarbons. He also carried out countless computer calculations for me, as did my research assistants through the years, Annette Knox, Mary Connolly, Laurie Stenberg, and Christine Owens. I am grateful for all of their help in sifting through endless mountains of papers and computer output. Thanks are also due Vitalii Pokrovskii for many helpful discussions and for generating Figures 11, 12, and 16, Christine Owens for bringing order out of chaos by supervising the delicate balancing act that is involved in writing organic/inorganic reactions among minerals and hydrocarbons, Barbara Ransom, Jan Amend, Everett Shock, and Leigh Price for many discussions of diagenetic systems and organic reactions, Rebecca Arington for drafting the figures, Joachim Hampel for photographing them, and last but not least, Joan Bossart for her incredible talent at translating my handwriting into the word processor with flawless precision and unflagging dedication. The manuscript benefited from reviews by George Skippen, Bernard Boudreau, and Robert Martin. Financial support was supplied by the National Science Foundation (NSF Grant EAR 8606052), the Department of Energy (DOE Grant DE-FG03-85ER-13419), and The Committee on Research at the University of California, Berkeley, all of which is acknowledged with thanks.

References

Amend, J.P. & Helgeson, H.C. (1991): Calculation of the relative stabilities at elevated temperatures and pressures of aqueous nucleosides, nucleotides, and other biochemical molecules required for bacterial metabolism in diagenetic processes. *Geol. Soc. Am., Abstr. Programs* **23**(5), A212.

Anderko, A. & Pitzer, K.S. (1991): Equation of state for pure fluids and mixtures based on a truncated virial expansion. *AIChE J.* **37**, 1379.

Arden, B.W. & Astill, K.N. (1970): *Numerical Algorithms: Origins and Applications*. Addison-Wesley, Reading, Massachusetts.

BARKER, J.A., ed. (1963): *Lattice Theories of the Liquid State*. Pergamon Press, Oxford, U.K.

BARTH, T. (1991): Organic acids and inorganic ions in waters from petroleum reservoirs, Norwegian continental shelf: a multivariate statistical analysis and comparison with American reservoir formation waters. *Appl. Geochem.* **6**, 1-15.

BERMAN, R.G. & BROWN, T.H. (1985): Heat capacity of minerals in the system Na_2O–K_2O–CaO–MgO–FeO–Fe_2O_3–Al_2O_3–SiO_2–TiO_2–H_2O–CO_2: representation, estimation, and high temperature extrapolation. *Contrib. Mineral. Petrol.* **89**, 168-183.

BESTOUGEFF, M.A. (1967): Petroleum hydrocarbons. *In* Fundamental Aspects of Petroleum Geochemistry (B. Nagy & U. Colombo, eds.), Elsevier, Amsterdam (77-108).

BIEDERMAN, E.W. (1986): *Atlas of Selected Oil and Gas Reservoir Rocks from North America*. J. Wiley & Sons, Inc., New York.

BOWERS, T.S. & HELGESON, H.C. (1983): Calculation of the thermodynamic and geochemical consequences of nonideal mixing in the system H_2O–CO_2–NaCl on phase relations in geologic systems: equation of state for H_2O–CO_2–NaCl fluids at high pressures and temperatures. *Geochim. Cosmochim. Acta* **47**, 1247-1275.

BRUTON, C.J. & HELGESON, H.C. (1983): Calculation of the chemical and thermodynamic consequences of differences between fluid and geostatic pressure in hydrothermal systems. *Am. J. Sci.* **283A**, 540-588.

CAROTHERS, W.W. & KHARAKA, Y.K. (1978): Aliphatic acid anions in oil field waters – implications for origin of natural gas. *Am. Assoc. Petrol. Geol. Bull.* **62**, 2441-2453.

CROSSEY, L.J., SURDAM, R.C. & LAHANN, R. (1986): Application of organic/inorganic diagenesis to porosity prediction. *In* Roles of Organic Matter in Sediment Diagenesis (D.L. Gautier, ed.). *Soc. Econ. Paleont. Mineral., Spec. Publ.* **38**, 147-155.

CUNNINGHAM, J.R. (1974): *Calculation of Parameters from Group Contributions for the PFGC Equation of State*. M.Sc. thesis, Brigham Young University, Provo, Utah.

DES MARAIS, D.J. & TRUESDELL, A.H. (1991): Carbon isotope geochemistry of individual hydrocarbons in springs and fumaroles of Yellowstone National Park, Wyoming. *Geol. Soc. Am., Abstr. Programs* **23**(5), A19.

DOBNER, A.B., GRAF, W., HAHN-WEINHEIMER, P. & HIRNER, A. (1978): Stable carbon isotopes of graphite from Bogola mine, Sri Lanka. *Lithos* **11**, 251-255.

DRUMMOND, S.E. & PALMER, D.A. (1986): Thermal decarboxylation of acetate. II. Boundary conditions for the role of acetate in the primary migration of natural gas and the transportation of metals in hydrothermal systems. *Geochim. Cosmochim. Acta* **50**, 825-834.

EYRING, H. (1936): Viscosity, plasticity, and diffusion as examples of absolute reaction rates. *J. Chem. Phys.* **4**, 283-291.

FEI, Y. & SAXENA, S.K. (1987): An equation for the heat capacity of solids. *Geochim. Cosmochim. Acta* **51**, 251-254.

FISHER, J.B. (1987): Distribution and occurrence of aliphatic acid anions in deep sub-surface waters. *Geochim. Cosmochim. Acta* **51**, 2459-2468.

FRENCH, B.M. (1964): *Stability of Siderite, $FeCO_3$, and Progressive Metamorphism of Iron Formation*. Ph.D. dissertation, The Johns Hopkins University, Baltimore, Maryland.

GOFFÉ, B. & VILLEY, M. (1984): Texture d'un matériel carboné impliqué dans un métamorphisme haute pression – basse température (Alpes françaises). Les hautes pressions influencent-elles la carbonification? *Bull. Minéral.* **107**, 81-91.

GREENWOOD, H.J. (1962): Synthesis and stability of anthophyllite. *Carnegie Inst. Wash. Yearbook* **61**, 85-88.

HAAS, J.L. & FISHER, J.R. (1976): Simultaneous evaluation and correlation of thermodynamic data. *Am. J. Sci.* **276**, 525-545.

HANOR, J.S. & WORKMAN, A.L. (1986): Distribution of dissolved volatile fatty acids in some Louisiana oil field brines. *Appl. Geochem.* **1**, 37-46.

HELGESON, H.C. (1970): A chemical and thermodynamic model of ore deposition in hydrothermal systems. *In* Fiftieth Anniversary Symposium (B.A. Morgan, ed.). *Mineral. Soc. Am., Spec. Pap.* **3**, 155-186.

_____ (1991): Thermodynamic constraints on the geobiochemical evolution of petroleum in the Earth's crust. *Geol. Soc. Am., Abstr. Programs* **23**(5), A25.

_____ (1992): Calculation of the thermodynamic properties and relative stabilities of aqueous acetic and chloroacetic acids, acetate and chloroacetates, and acetyl and chloroacetyl chlorides at high and low temperatures and pressures. *Appl. Geochem.*, in press.

_____, DELANY, J.M., NESBITT, W.H. & BIRD, D.K. (1978): Summary and critique of the thermodynamic properties of rock-forming minerals. *Am. J. Sci.* **278A**.

_____ & KIRKHAM, D.H. (1976): Theoretical prediction of the thermodynamic behavior of aqueous electrolytes at high pressures and temperatures. III. Equation of state for aqueous species at infinite dilution. *Am. J. Sci.* **276**, 97-240.

_____, _____ & FLOWERS, G.C. (1981): Theoretical prediction of the thermodynamic behavior of aqueous electrolytes at high pressures and temperatures. IV. Calculation of activity coefficients, osmotic coefficients and apparent molal and standard and relative partial molal properties to 600°C and 5 kbar. *Am. J. Sci.* **281**, 1249-1516.

_____, KNOX, A.M. & SHOCK, E.L. (1991): Petroleum, oil field brines, and authigenic mineral assemblages: are they in metastable equilibrium in hydrocarbon reservoirs? *15th Int. Meet., Eur. Assoc. Org. Geochem., Program Abstr.*, 39.

_____ & SHOCK, E.L. (1988): Role of oxidation/reduction reactions in the hydrothermal transport and deposition of petroleum. *Geol. Soc. Am., Abstr. Programs* **20**(7), A95.

HENDRICKSON, J.B., CRAM, D.J. & HAMMOND, G.S. (1970): *Organic Chemistry* (3rd ed.). McGraw-Hill, New York.

HOLDAWAY, M.J. & GOODGE, J.W. (1990): Rock pressure versus fluid pressure as a controlling influence on mineral stability: an example from New Mexico. *Am. Mineral.* **75**, 1043-1058.

HOLLAND, T.J.B. & POWELL, R. (1990): An enlarged and updated internally consistent thermodynamic data set with uncertainties and correlations: the system K_2O–Na_2O–CaO–MgO–FeO–Fe_2O_3–Al_2O_3–TiO_2–SiO_2–C–H_2–O_2. *J. Metamorph. Geol.* **8**, 89-124.

HOLLOWAY, J.R. (1977): Fugacity and activity of molecular species in supercritical fluids. *In* Thermodynamics in Geology (D. Fraser, ed.). D. Reidel, Boston (161-181).

HOWER, J., ESLINGER, E., HOWER, M.E. & PERRY, E.A. (1976): Mechanism of burial metamorphism of argillaceous sediment 1. Mineralogical and chemical evidence. *Geol. Soc. Am. Bull.* **87**, 725-737.

HUNT, J.M. (1979): *Petroleum Geochemistry and Geology*. W.H. Freeman & Co., San Francisco, California.

JOHNSON, J.W. & NORTON, D. (1991): Critical phenomena in hydrothermal systems: state, thermodynamic, electrostatic, and transport properties of H_2O in the critical region. *Am. J. Sci.* **291**, 541-648.

_____, OELKERS, E.H. & HELGESON, H.C. (1992): SUPCRT92: software package for calculating the standard molal thermodynamic properties of minerals, gases, aqueous species, and reactions from 1 to 5000 bars and 0° to 1000°C. *Comput. & Geosci.* (in press).

KELLEY, K.K. (1960): Contributions to the data on theoretical metallurgy. XIII. High temperature heat content, heat capacity and entropy data for the elements and inorganic compounds. *U.S. Bur. Mines, Bull.* **584**.

KHARAKA, Y.K., CALLENDER, E. & CAROTHERS, W.W. (1977): Geochemistry of geopressured geothermal waters from the Texas Gulf Coast. *Proc. 3rd Geopressured-Geothermal Energy Conference (Univ. Southwestern Louisiana, Lafayette, Louisiana)*, GI-121 – GI-155.

_____, LAW, L.M., CAROTHERS, W.W. & GOERLITZ, D.F. (1986): Role of organic species dissolved in formation waters from sedimentary basins in minerals diagenesis. *In* Roles of Organic Matter in Sediment Diagenesis (D.L. Gautier, ed.). *Soc. Econ. Paleont. Mineral., Spec. Publ.* **38**, (111-122).

KINGHORN, R.F.K. (1983): *An Introduction to the Physics and Chemistry of Petroleum*. Wiley, New York, N.Y.

LEVINE, J.R., SAMSON, I.M. & HESSE, R. (1991): Occurrence of fracture-hosted impsonite and petroleum fluid inclusions, Quebec City region, Canada. *Am. Assoc. Petrol. Geol. Bull.* **75**, 139-155.

MACGOWAN, D.B. & SURDAM, R.C. (1987): The role of carboxylic acid anions in formation waters, sandstone diagenesis and petroleum reservoir modeling. *Geol. Soc. Am., Abstr. Programs* **19** (7), 753.

_____ & _____ (1988): Difunctional carboxylic acid anions in oilfield waters. *Org. Geochem.* **12**, 245-259.

_____ & _____ (1990a): Carboxylic acid anions in formation waters, San Joaquin Basin and Louisiana Gulf Coast, U.S.A. – implications for clastic diagenesis. *Appl. Geochem.* **5**, 687-701.

_____ & _____ (1990b): Importance of organic–inorganic reactions to modeling water–rock interactions during progressive clastic diagenesis. *In* Chemical Modeling of Aqueous Systems II (D.C. Melchior & R.L. Bassett, eds.). *Am. Chem. Soc., Symp. Ser.* (494-507).

MAIER, C.G. & KELLEY, K.K. (1932): An equation for

the representation of high temperature heat content data. *Am. Chem. Soc. J.* **54**, 3243-3246.

MAIR, B.J. (1964): Hydrocarbons isolated from petroleum. *Oil and Gas J.* **62**(37), 130-134.

MAJEED, A.I. & WAGNER, J. (1986): Parameters from group contributions equation and phase equilibria in light hydrocarbon systems. *In* Equations of State: Theories and Applications (K.C. Chao & R.L. Robinson, Jr., eds.). *Am. Chem. Soc., Symp. Ser.* **300**, 452-473.

MEANS, J.L. & HUBBARD, N. (1987): Short-chain aliphatic acid anions in deep subsurface brines: a review of their origin, occurrence, properties, and importance and new data on their distribution and geochemical implications in the Palo Duro Basin, Texas. *Org. Geochem.* **11**, 177-191.

MILLER, S.L. & BADA, J.L. (1988): Submarine hot springs and the origin of life. *Nature* **334**, 609-611.

NORTH, F.K. (1985): *Petroleum Geology.* Allen and Unwin, Boston, Massachusetts.

PALMER, D.A. & DRUMMOND, S.E. (1986): Thermal decarboxylation of acetate. I. The kinetics and mechanism of reaction in aqueous solution. *Geochim. Cosmochim. Acta* **50**, 813-824.

PENG, D.-Y. & ROBINSON, D.B. (1976): A new two-constant equation of state. *Ind. Eng. Chem. Fundam.* **15**, 59-64.

PETER, J.M., PELTONEN, P., SCOTT, S.D., SIMONEIT, B.R.T. & KAWKA, O.E. (1991): ^{14}C ages of hydrothermal petroleum and carbonate in Guaymas Basin, Gulf of California: implications for oil generation, expulsion, and migration. *Geology* **19**, 253-256.

PITZER, K.S., PEIPER, J.C. & BUSEY, R.H. (1984): Thermodynamic properties of aqueous sodium chloride solutions. *J. Phys. Chem. Ref. Data* **13**, 1-102.

PRAUSNITZ, J.M., LICHTENTHALER, R.N. & DE AZEVEDO, E.G. (1986): *Molecular Thermodynamics of Fluid-Phase Equilibria* (2nd ed.). Prentice-Hall, Englewood Cliffs, New Jersey.

PRICE, L.C. (1982): Organic geochemistry of core samples from an ultradeep hot well (300°C, 7 km). *Chem. Geol.* **37**, 215-228.

_____ (1983): Geologic time as a parameter in organic metamorphism and vitrinite reflectance as an absolute paleogeothermometer. *J. Petrol. Geol.* **6**, 5-38.

_____ (1991): Hydrocarbon thermal stability as a maximum indicator of bacterial endurance down the geotherm? *Geol. Soc. Am., Abstr. Programs* **23**(5), A20.

_____, CLAYTON, J.L. & RUMEN, L.L. (1979): Organic geochemistry of a 6.9-kilometer-deep well, Hinds County, Mississippi. *Trans. Gulf Coast Assoc. Geol. Soc.* **29**, 352-370.

_____, _____ & _____ (1981): Organic geochemistry of the 9.6 km Bertha Rogers No.1 well, Oklahoma. *Org. Geochem.* **3**, 59-77.

_____, DAWS, T. & PAWLEWICZ, M. (1986): Organic metamorphism in the Lower Mississippian - Upper Devonian Bakken shales. 1. Rock-val pyrolysis and vitrinite reflectance. *J. Petrol. Geol.* **9**(2), 125-162.

PRIGOGINE, I. & DEFAY, R. (1954): *Chemical Thermodynamics.* Longmans, Green and Co., Ltd., London.

REVERDATTO, V.V., MENELEVSKIY, V.N. & MELAMED, V.G. (1984): Time and temperature as factors of hydrocarbon generation in the contact metamorphism of rocks containing dispersed organic matter: the case of parallel basalt sills. *Dokl. Akad. Nauk SSSR (1982)* **266**(4), 952-955.

RUMBLE, D., III, CHAMBERLAIN, C.P., ZEITLER, P.K. & BARREIRO, B. (1989): Hydrothermal graphite veins and Acadian granulite facies metamorphism, New Hampshire, USA. *In* Fluid Movements - Element Transport and the Composition of the Deep Crust (D. Bridgwater, ed.). Kluwer Academic Publishers, Amsterdam, The Netherlands.

_____, DUKE, E.F. & HOERING, T.C. (1986): Hydrothermal graphite in New Hampshire: evidence of carbon mobility during regional metamorphism. *Geology* **14**, 452-455.

_____ & HOERING, T.C. (1986): Carbon isotope geochemistry of graphite vein deposits from New Hampshire, U.S.A. *Geochim. Cosmochim. Acta* 50, 1239-1247.

SASSEN, R., MCCABE, C., KYLE, J.R. & CHINN, E.W. (1989): Deposition of magnetic pyrrhotite during alteration of crude oil and reduction of sulfate. *Org. Geochem.* **14**, 381-392.

SATO, M. (1990): Thermochemistry of the formation of fossil fuels. *In* Fluid-Mineral Interactions: a Tribute to H.P. Eugster (R.J. Spencer & I-Ming Chou, eds.). *Geochem. Soc., Spec. Publ.* **2**, 271-283.

SCHREIBER, D.R. & PITZER, K.S. (1989): Equation of state in the acentric factor system. *Fluid Phase Equilibria* **46**, 113-130.

SHOCK, E.L. (1987): Metastable equilibria among minerals and organic aqueous species in the

diagenetic environment. *Geol. Soc. Am., Abstr. Programs* **19**(7), 842.

_____ (1988): Organic acid metastability in sedimentary basins. *Geology* **16**, 886-890.

_____ (1990a): Do amino acids equilibrate in hydrothermal fluids? *Geochim. Cosmochim. Acta* **54**, 1185.

_____ (1990b): Stability of peptides in high temperature aqueous solutions. *Geol. Soc. Am., Abstr. Programs* **22**(7), A158.

_____ (1990c): Geochemical constraints on the origin of organic compounds in hydrothermal systems. *In* Origins of Life and Evolution of the Biosphere. Kluwer Academic Publishers, Amsterdam, The Netherlands (331-367).

_____ (1991): Hydrothermal dehydration. *Geol. Soc. Am., Abstr. Programs* **23**(5), A25.

_____ & HELGESON, H.C. (1986): Thermodynamic properties of aqueous organic species in the diagenetic environment. *Geol. Soc. Am., Abstr. Programs* **18**(6), 749.

_____ &_____ (1988): Calculation of the thermodynamic and transport properties of aqueous species at high pressures and temperatures: correlation algorithms for ionic species and equation of state predictions to 5 kb and 1000°C. *Geochim. Cosmochim. Acta* **52**, 2009-2036.

_____ & _____ (1990): Calculation of the thermodynamic and transport properties of aqueous species at high pressures and temperatures: standard partial molal properties of organic species. *Geochim. Cosmochim. Acta* **54**, 915-945.

_____, _____ & SVERJENSKY, D.A. (1989): Calculation of the thermodynamic and transport properties of aqueous species at high pressures and temperatures: standard partial molal properties of inorganic neutral species. *Geochim. Cosmochim. Acta* **53**, 2157-2183.

_____, OELKERS, E.H., JOHNSON, J.W., SVERJENSKY, D.A. & HELGESON, H.C. (1992): Calculation of the thermodynamic properties of aqueous species at high pressures and temperatures: effective electrostatic radii, dissociation constants, and standard partial molal properties to 1000°C and 5 kb. *J. Chem. Soc. London, Faraday Trans.*, in press.

SIMONEIT, B.R.T. (1990): Petroleum generation, an easy and widespread process in hydrothermal systems: an overview. *Appl. Geochem.* **5**(1/2), 3-16.

_____ (1991): Aqueous high temperature and high pressure organic geochemistry. *Geol. Soc. Am., Abstr. Programs* **23**(5), A19.

_____, BRAULT, M. & SALIOT, A. (1990): Hydrocarbons associated with hydrothermal minerals, vent waters and talus on the East Pacific Rise and Mid-Atlantic Ridge. *Appl. Geochem.* **5** (1/2), 115-124.

_____, BRENNER, S., PETERS, K.E. & KAPLAN, I.R. (1981): Thermal alteration of Cretaceous black shale by diabase intrusions in the eastern Atlantic. II. Effects on bitumen and kerogen. *Geochim. Cosmochim. Acta* **45**, 1581-1602.

STUART, C.A. (1970): Geopressures. *Suppl. Proc. 2nd Symp. on Abnormal Surface Pressures (Louisiana State Univ., Baton Rouge, Louisiana)*, 121.

SVERJENSKY, D.A. (1984): Oil field brines as ore-forming solutions. *Econ. Geol.* **79**, 23-37.

TANGER, J.C., IV & HELGESON, H.C. (1988): Calculation of the thermodynamic and transport properties of aqueous species at high pressure and temperatures: revised equations of state for the standard partial molal properties of ions and electrolytes. *Am. J. Sci.* **288**, 19-98.

THOMAS, E.R. & ECKERT, C.A. (1984): Prediction of limiting activity coefficients by a modified separation of cohesive energy density model and UNIFAC. *Ind. Eng. Chem. Process Des. Dev.* **23**, 194-209.

TISSOT, B.P. & WELTE, D.H. (1984): *Petroleum Formation and Occurrence* (2nd ed.). Springer-Verlag, Berlin.

WEIS, P., FRIEDMAN, I. & GLEASON, J.D. (1981): The origin of epigenetic graphite: evidence from isotopes. *Geochim. Cosmochim. Acta* **45**, 2325-2332.

WILLEY, L.M., KHARAKA, Y.K., PRESSER, T.S., RAPP, J.B. & BARNES, I. (1975): Short chain aliphatic acid anions in oil field waters and their contribution to the measured alkalinity. *Geochim. Cosmochim. Acta* **39**, 1707-1711.

WILSON, G.M. (1972): Flory–Huggins entropy, effect of liquid expansion. *Center for Thermochemical Studies, Brigham Young Univ. (Provo, Utah), Contrib.* **34**.

WORKMAN, A.L. & HANOR, J.S. (1985): Evidence for large-scale vertical migration of dissolved fatty acids in Louisiana oil field brines: Iberia field, south-central Louisiana. *Trans. Gulf Coast Assoc. Geol. Soc.* **35**, 293-300.

Received March 11, 1991, revised manuscript accepted November 29, 1991.